Université de Montréal

# Newly-developed Parameters to Quantify Texture:
# Application to Polymeric Porous Structures

par

Ashraf Alsadat Hashemi Sangdehi

Faculté de pharmacie

Mémoire présenté à la Faculté des études supérieures
en vue de l'obtention du grade de
Maîtrise en sciences
en Sciences pharmaceutiques
Option technologie pharmaceutique

Janvier 2005
© Ashraf Alsadat Hashemi Sangdehi, 2005

Université de Montréal

Faculté des études supérieures

Ce mémoire intitulé:

# Newly-developed Parameters to Quantify Texture:
# Application to Polymeric Porous Structures

Présenté par :

Ashraf Alsadat Hashemi Sangdehi

A été évalué par un jury composé des personnes suivantes :

Dr Louis Cartilier, président-rapporteur
Dr Fahima Nekka, directeur de recherche
Dr Patrice Hildgen, membre du jury
Dr Bernard Goulard, membre du jury

# Résumé

La connaissance de la structure poreuse des matériaux hétérogènes est d'une importance fondamentale puisque leurs propriétés physiques en dépendent largement. En effet, les caractéristiques géométriques et structurales des matériaux poreux influencent leur performance, plus particulièrement les propriétés de diffusivité et de perméabilité des matériaux polymériques.

Ce mémoire de maîtrise s'inscrit dans un effort collectif visant à étudier, au-delà de la porosité, les propriétés morphologiques des matériaux poreux. L'outil principal de notre étude était la fonction d'autocorrélation (FAC), largement répandue dans l'analyse du signal. Nous avons revisité cette méthode et proposé une manière originale de l'employer dans un contexte géométrique (spatial au lieu de temporel) afin d'extraire de l'information morphologique des structures étudiées. Nous avons illustré sur des exemples, comment la méthode développée peut être utilisée comme complément à la porosité.

La première étape de cette étude était d'appliquer la fonction d'autocorrélation aux images biphasées. Nous avons alors prouvé empiriquement que la pente en moyenne quadratique (LMS) de cette fonction d'autocorrélation est égale à la porosité de ces textures. Dans la troisième étape, cette information de porosité du signal de la fonction d'autocorrélation est soustraite afin de ne maintenir que l'information géométrique complémentaire. Cette action de soustraction a aussi un intérêt purement technique puisqu'elle permet d'épurer le signal et ainsi de mieux le préparer à la quatrième étape, c'est à dire à l'application de la transformée de Fourier. Le signal résultant de cette dernière opération a été alors analysé pour en extraire d'autres informations structurales. Ainsi, deux paramètres indépendants ont été trouvés et définis par les composants de "pente" et d'"oscillation" du spectre de la fonction d'autocorrélation. Dans le cas des images rayées et des images avec les modèles périodiques, la fréquence principale de la transformée de Fourier en termes de l'amplitude a été liée à la fréquence et à l'ampleur des pores. Cette technique, qui est développée pour l'étude des textures poreuses, s'annonce prometteuse et mérite d'être développée davantage dans des situations plus générales. À notre connaissance, cette étude constitue la première du genre où la fonction d'autocorrélation est

utilisée de la sorte dans l'étude des structures géométriques. Sa généralisation à des structures plus générales est en cours de développement par d'autres membres de mon laboratoire.

# Abstract

Distinguishing porous microstructures in a quantitative manner is important for reliable predictions of their properties. Indeed, the geometric and structural properties of porous materials influence their performance, especially the diffusivity and permeability of polymeric materials. The purpose of this M.Sc. thesis is to characterize, beyond porosity, the morphological properties of porous structures. The main tool is the autocorrelation function (ACF), a widely-used signal analysis. We revisited this method and proposed an original way for its analysis in order to reveal the morphology of porous media by developing parameters that quantify texture. In fact, we showed how our developed method can contribute to a better description of texture and set apart surfaces of materials that are indistinguishable by other parameters such as porosity. As a first step, we applied the autocorrelation function to 2-phase images. The second step consisted of establishing an experimental proof that the least mean square slope of this autocorrelation function was directly related to the porosity of these textures. In the third step, this porosity information from the autocorrelation function signal was removed to keep only complementary geometric information of the image. This subtraction purified the signal and prepared it for the fourth step, i.e. discrete Fourier transform (DFT) application to the remaining part. The resulting signal was then analyzed to extract other structural information. Thus, 2 important independent parameters were found, studied, and defined through the "slope" and "oscillation" components of the autocorrelation function. In the case of striped images, i.e. images with periodic patterns, the main frequency of the DFT in terms of amplitude was related to pore frequency and extent. This technique, designed for the study of porous textures, is promising and calls for further development. To the best of our knowledge, it is the first time that the autocorrelation function has been applied this way. Its generalization to more porous media is under development by other members of our laboratory.

# Table of Contents

# List of tables

# List of figures

# Abbreviations and symbols

| | |
|---|---|
| × | operation for multiplication group |
| Ln | logarithmic function |
| $\int$ | integration symbol |
| $\Pi$ | product symbol |
| $\Sigma$ | summation symbol |
| $\langle\ \rangle$ | the average over a function |
| ACF | the autocorrelation function |
| FT | Fourier transform |
| DFT | discrete Fourier transform |
| FFT | fast Fourier transform |
| $V_{ads}$ | molar volume of the adsorbate |
| $S/V$ | surface area to volume ratio |
| $\partial P$ | pore space |

| | |
|---|---|
| $\partial S$ | matrix space |
| $\phi(S)$ | porosity of a porous medium |
| $V_3(P)$ | volume fraction of pore space |
| $V_3(S)$ | volume of total sample |
| $L_i$ | volume of cubic sample |
| $a_i$ | length of capillary tubes |
| $N$ | number of capillary tubes, the total number of samples in Fourier transform |
| $P$ | pressure |
| $\delta$ | surface tension of mercury |
| $\theta$ | contact angle of mercury on the material |
| D | diameter of assumed aligned cylinders |
| $J$ | filtration rate |
| $n$ | number of pores per $cm^2$ |

| | |
|---|---|
| $A$ | surface area of the polymeric sample |
| $R$ | pore radius |
| $\eta$ | viscosity of the flow |
| $\tau$ | thickness |
| $r_0 / r_m$ | ratio of the smallest radius to the largest pore |
| $D$ | fractal dimension |
| $N$ | number of iterations |
| $N_n$ | number of segments in the Cantor set |
| $l_n, L_n$ | length of segments in the Cantor set |
| $l_k$ | length of holes in the Cantor set |
| $NP(n)$ | possible number of mixed fractals |
| $A$ | scale of box size or iteration |
| $L_{la}$ | lacunarity |
| $E(S)$ | mean of box mass values |

| | |
|---|---|
| $var(S)$ | variance of box mass values |
| $H^s$ | Hausdorff measure |
| $I^{sh(t)}$ | Hausdorff measure function spectrum (HMFS) |
| $t$ | shift point |
| $\chi_F$ | indicator function representing the structure as a special signal |
| $X(f)$ | Fourier transform |
| $\mathbf{f}, f, f_0$ | frequency, possibly for the continuous signal, for the periodic signal |
| $T_0$ | duration in Fourier transformation |
| $K$ | Spectral domain index |
| $x(t), f(x), g(x)$ | characteristic functions |
| $y(t), I(t)$ | Product of correlation of 2 functions |
| $C(i)$ | the $i^{th}$ component of the autocorrelation vector |
| $a_{j,k}, b_{j,k}$ | the image matrix |

*To my parents and my husband*

# Acknowledgements

I wish to acknowledge my supervisor, Prof. Fahima Nekka, for her helpful suggestions, vast knowledge, support and constant encouragement throughout this work. I truly appreciate her positive guidance, 'open door' policy and patience.

I thank Professor Patrice Hildgen for allowing me to use his lab facilities at the beginning of this thesis. I greatly appreciate his help when nothing seemed to work.

I also thank Dr. Jun Li for his time and effort to explain the fundamental concepts of the present work to me.

I express my gratitude to Corentin Dubois, a trainee in Professor Nekka's lab, from École Centrale de Nantes, who helped me to understand many tricks in programming.

My sincerest and deepest thanks are due to my husband, Mehdi Aarabi. I never forget that this work could not have been accomplished without his encouragement, support and love. My heartful thanks go to my parents, brothers and sister, for offering their unconditional love and support.

I would also like to express my gratitude to my parents- and brothers-in-law, who have followed my academic career and have always been encouraging.

# CHAPTER 1: INTRODUCTION

# Heterogeneous media

Most multi-phase media have a random microstructure with inclusions of different sizes and shapes forming an enormous variety of local microstructural configurations. The composition of an heterogeneous material varies from region to region, where the distance between regions may range from microns upwards. However, it has been shown that the effective macroscopic properties of heterogeneous materials are not related in a simple way to the properties of the constitutive phases and their related proportions, which suggest complex interactions between phases.

Porous polymers, as an important subclass of heterogeneous materials, have been used in a variety of applications, including chromatographic media (Zeng et al., 2004), controlled release of drugs (Risbud et al., 2000) and wound dressing (Pachence, 1996; Shibata et al., 1997). Although the presence of pores is a major defect in metals (Huang and Lu, 2002) that can compromise their mechanical properties due to cracking and fatigue, porosity also has an important influence on the diffusivity and permeability of porous media. To characterize a porous structure, porosity is considered as a principal index reflecting its spatial occupancy. However, it is obvious that porosity alone is far from enough to reflect the irregular morphology of microporous structures. The properties of porous media are highly dependent on the morphology of pore space as well as of its complementary part. To go one step further in the characterization process, complementary parameters have to be extracted.

The purpose of this chapter is to report on the problems and limitations associated with the characterization techniques of porous media. We will also justify the need to develop more advanced methods to more fully characterize porous structures.

## Characterization of porous media

Porous media are generally characterized by a number of geometric parameters. The most common are porosity, surface area, and pore size distribution (Hilfer & Manwart, 2001; Hilfer, 2002). In an effort to explicitly study these structures, a number

of important analytical and empirical techniques have been developed. Each of these techniques has its own set of strengths and weaknesses.

To be efficient, geometric parameters for the characterization of porous media should satisfy some important requirements (Carman, 1956; Hilfer, 1996), that is, the parameters should be well-defined, directly predictive in an experiment, not require too much data, and be readily usable.

We should also mention the fractal approach (Krohn & Thompson, 1986; Yu & Li, 2001), which is intended to quantify structures of high complexity. Fractal dimension, which can be viewed as a measure of structure irregularity, gives a first characterization of such microstructures. Several methods have been proposed to measure the dimension of a fractal, or, more generally, of an irregular set. However, one major limitation of fractal dimension is that it can degenerate, meaning that several sets can share the same fractal dimension, while exhibiting different textures. The notion of lacunarity, which is related to the distribution of mass and voids in a set (Allain & Cloitre, 1991), has been proposed as a promising way to differentiate textures beyond fractal dimension. However, in many cases, this index is not sufficient to add complementary information since it can also degenerate in rather simple cases (Nekka & Li, 2003b). In the following, the above-mentioned characterization methods are presented, as are some experimental techniques.

## Porosity

The study of porous media mainly involves porosity, which refers to the occupancy of the set, measured on samples having regular geometric shapes (Nekka et al., 2005). The porosity of a structure is defined as the ratio of the volume of pores to the volume of the material. Hence, a 2-component sample with pore space $\partial P$ (component 1) and matrix space $\partial S$ (component 2) has a porosity of:

$$\phi = \frac{V_3(\partial P)}{V_3(\partial S)}$$

where $V_3(\partial P)$ is the volume fraction of pore space, while $V_3(\partial S)$ is the volume of the total sample. It should be mentioned that this definition of porosity is related to total porosity. The latter differs from open porosity or effective porosity, which is the ratio of accessible pore volume (i.e. of pores connected to the surface of the sample) to total volume. Several methods, such as mercury porosimetry and small-angle neutron/x-ray scattering, experimentally measure the porosity of a porous medium. Some of them will be discussed in the next section.

## Specific internal surface area

Porous materials have a large surface area, and the behaviour of fluids through pores is dominated by surface forces. This concept introduces another important geometric characteristic of porous media, which gives a quantitative measure of the surface area to volume (S/V) ratio. Experimental surface area methods are generally based on analysis of adsorption isotherms of nitrogen or some other gas. One of the important techniques, the Brunauer-Emmett-Teller (BET) method (Thomas et al., 1999), will be discussed, along with other experimental methods, in the next section.

## The correlation function (CF)

Based on the quantification of relationships in a given sample over a range of length scales (Berryman, 1987), the CF offers another geometric method for the characterization process. Its advantage lies in the fact that, in combination with other characterization methods, such as porosity and surface area, it has the potential of a quantitative textural technique (Hilfer, 1996) for heterogeneous and disordered materials. Correlations can be established over a wide variety of functions, such as the radial distribution of spheres (Markov & Willis, 1998) and localized change in density. This function has the advantage of being easy to manipulate, and provides deep insight into

texture. The method we propose is based on the autocorrelation function (ACF), a special version of the CF. We will discuss the ACF in more detail in the Methodology section.

## Pore size distribution

Pore size distribution on structures is very useful information. However, its definition can be problematic, since it necessitates the selection of pore shape definition. Mercury porosimetry is an important procedure to determine pore size distribution. The technique may be fraught with small approximations introduced to make the models tractable. Indeed, pores are usually assumed to be either slit-shaped or cylindrical, leading to a single variable size parameter (wall spacing or cylinder radius).

## Capillary tubes

Continuous pore spaces between the matrix act like capillary tubes. The capillary tube model (Hilfer, 1996) is a simple geometric approach to the specific geometric characterization of porous media. The idea is based on the consideration of porous spaces in an assumed cubic porous structure as bundles of straight or parallel cylindrical tubes that do not intersect each other (Figure 1.1).
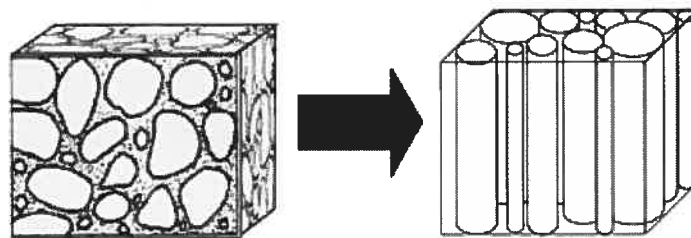


Figure 1.1: Pore geometry presented by a bundle of parallel tubes[1]

Therefore, porosity in a cubic porous model with side length $L$ and volume $L_i$ consists of $N$ non-intersecting capillary tubes of length $a_i$ which have circular cross sections defined by:

$$\phi(S) = \frac{2\pi}{L^3} \sum_{i=1}^{N} L_i a_i$$

## Experimental techniques for porosity and surface area

Several experimental techniques for the characterization of porous materials are briefly described below to get an idea of their associated forces and/or limits.

- **Chemical gas adsorption:** used for the determination of surface area (BET method), micropore volume and pore size distribution;
- **Mercury porosimetry:** serves to estimate bulk or apparent density and macropore volume;
- **Small-angle x-ray scattering (SAXS):** characterizes porous materials in terms of surface area, total pore volume and pore size distribution;
- **Nuclear magnetic resonance (NMR) spectroscopy:** measures the S/V ratio.

The choice of the optimization method depends, however, upon the problem under study and requires execution efficiency. Each of these techniques measures the surface area of material pores by different physical principles. Unfortunately, each technique can give a different surface area value.

- **Chemical gas adsorption**

This widely-used technique is by far the oldest way of measuring surface area, pore size distribution and total pore volume, including pores with diameters smaller than 100 nm. The physical principle of the technique is detailed in a book by Lowell & Shields (1991). The concept is based on the tendency of all solid surfaces to attract

surrounding gas molecules. Generally, nitrogen vapour is the sorptive gas (Pinnau et al., 1992). The sorptive gas slowly goes through the specimen, and the amount of adsorbed nitrogen, measured as a function of applied vapour pressure, is finally reported as the adsorption isotherm. The BET method is the most widely-used. It is based on the assumption that the heat of adsorption is constant throughout the formation of a single layer (monolayer) of nitrogen molecules on the surface. An important characteristic of the technique is that the specimen must be penetrated to remove all adsorbed gas molecules, and the subsequent measurement must be performed in a vacuum (Thomas et al., 1999), which limits its utility for amorphous materials. Its application to determine surface fractal dimension is presented later.

Salonen et al. (2000) compared the BET method to SAXS as a means of measuring the porosity and surface area of porous silicon. They found that when sample porosity was greater than 50%, the results obtained by both methods were similar. However, the BET method seems to give unrealistically large values for specific surface area when porosity is less than 50%.

- **Mercury porosimetry**

This method, proposed by Washburn in 1921, provides reliable information about pore size/volume distribution, particle size distribution, bulk density and specific surface for most porous solids, regardless of their nature and shape. It is based on the physical principle that a non-reactive, non-wetting liquid will not penetrate pores until sufficient pressure is applied to force its entry. Pore-size distribution is given by the so-called *Washburn equation* (Washburn, 1921):

$$P = \frac{4\delta \cos\theta}{d}$$

where $\delta$ is the surface tension of mercury, $\theta$ is the contact angle of mercury on the material being intruded under the required pressure $P$ to force mercury into the pore, and

$d$ is the diameter of a series of assumed aligned cylinders. Despite the widespread use of this method, it suffers from the main drawback that pores in a real porous medium are almost never circular cylinders (Xu et al., 2004).

Mercury porosimetry provides measurements of pore radii in the range of about several million down to 18 Angstroms. The size-limited property of meso- and macropores is another drawback of this method (Thomas et al., 1999). Moreover, it is generally not effective for aerogels. Indeed, the high compressive forces encountered in forcing mercury into aerogel pores and vacuum degassing to remove moisture cause these structures to collapse.

In addition to the above technique, Lee and Shim (1997) adopted the **Hagen-Poiseuille law** to measure the effective pore size of some types of polyamide membranes at various pH:

$$ J = \frac{n \pi r^4 A P}{8 \eta \tau} $$

where $J$ is the filtration rate, $n$ stands for the number of pores per $cm^2$, $A$ refers to the surface area of the polymeric sample ($cm^2$), $r$ is the pore radius, $P$ is the applied pressure, $\eta$ is the viscosity of the flow, and $\tau$ is the thickness of the membrane.

The drawback of this method is that it is only valid for laminar flow, and is based on the assumption that flow occurs when an incompressible, uniform viscous liquid (the so-called Newtonian fluid) passes through a cylindrical tube with a constant circular cross-section.

- ### Small-angle x-ray scattering (SAXS)

SAXS is based on the tendency of porous materials and nano-particles in an homogeneous matrix to scatter x-ray beams and the observation of a coherent scattering pattern that arises from electron density within a given sample. The angular scattering pattern is analyzed by the inverse relationship between particle sizes and scattering angle to distinguish characteristic shape and size features within the sample.

SAXS provides cutting edge capabilities for probing large length scale structures, such as polymers, biological macromolecules, meso- and nanoporous materials, and molecular self-assemblies (Wu, 2003). SAXS and neutron scattering can be applied to study both mono-disperse and poly-disperse systems to determine size distributions, volume fractions and total surface area. The main advantage of this method is that samples can be studied in a saturated state, thus avoiding possible problems associated with removing moisture. However, it has its own problems, mainly during data analysis. Variation of surface area values obtained from different instruments has been reported (Thomas et al., 1999). One possibility is the calibration of scattering intensity, which may give variations of up to 10% in surface area values. Also, the method is more valuable for mono-disperse systems than for poly-disperse systems, since size distribution is estimated on the assumption that all particles have the same shape.

## ▪ Nuclear magnetic resonance (NMR) spectroscopy

Non-invasive and non-destructive NMR spectroscopy, generally used to study molecular structures, provides important insights into the organization of porous materials (Freude & Karger, 2002). Based on liquid-infused diffusion measurement, the NMR method quantifies the S/V ratio. In porous material studies, the act of pumping water into solid pore walls is of great importance. The NMR relaxation time of water depends on pore size, is inversely proportional to the S/V ratio, and is thus directly related to pore radius (Rijniers et al., 2004).

A unique technique, called xenon inter-phase exchange NMR (Butler et al., 2002), has recently been developed to measure the S/V ratio of porous polymer samples. The advantage of this new method is the rapidity of gas diffusion and the long spin polarization lifetime.

# Fractal characteristics of porous media

The purpose of this section is to investigate fractal-based techniques to quantify porous images. Fractal geometry was popularized by Mandelbrot (1982) as a generalization of Euclidean geometry. Using concepts of fractal geometry, more complex structures with self-similar properties can be assessed. Porous structures and blood networks (Avnir et al., 1985; Gouyet, 1992) are typical real fractal systems, since they have a similar appearance over a range of scales. Fractal methods have already proved to be efficient in quantifying complex information based on existing similarities. The major use of fractal analysis is to measure this complexity through fractal dimension and other related indexes (Nekka et al., 2005).

Several studies based on wave-scattering or adsorption techniques (Avnir et al., 1985; Krohn & Thompson, 1986; Yu & Li, 2001) have shown that pore microstructures display self-similar features in terms of pore sizes and pore interface.

An interesting relationship (Hunt, 2003) between porosity $\phi$ and fractal dimension $D$ is expressed through:

$$\phi = 1 - (\frac{r_0}{r_m})^{3-D}$$

where $D$ is the (volume) fractal dimension of the pore space, and $r_0 / r_m$ is the ratio of the smallest to the largest pore radius in the sample. The negative sign implies that with increased pore size in the sample, the pore population decreases. In the typical case of vanishing porosity or a large $r_0 / r_m$ ratio, the limit of $D$ towards 3 corresponds to a filled cubic object without any pore inside. In general, $r_0 / r_m$ is $<10^{-2}$ for a porous medium with fractal properties; otherwise, the porous medium has a non-fractal structure, and fractal theory and techniques are not applicable (Yu & Cheng, 2002). Diverse available approaches estimate fractal dimension, depending on differences in objectives and types of data under study. Some of the basic techniques are presented below. Before going through some of them, I will discuss typical fractals, including fat fractals, known to be realistic synthetic models of porous media.

# Thin fractals: the typical example of the triadic Cantor set

Thin fractals are sets of zero-Lebesgue measure (length in 1-D). A typical example is the Cantor set. Let us recall the general construction of this set. At the zeroth level, construction begins with the unit interval. The first level is obtained from the zeroth level by deleting all points that lie in the middle third, that is, all points between 1/3 and 2/3. The second level is obtained by deleting the middle third of each remaining interval of the first level, that is, all points between 1/9 to 2/9 and 7/9 to 8/9. The process continues *ad infinitum*. The first 3 iterations are depicted in Figure 1.2 below.



**Figure 1.2: Initial unit interval and the first 3 iterations of construction of the triadic Cantor set**

At the $n^{th}$ level, the set consists of $N_n = 2^n$ segments, each of which has length $l_n = 1/3^n$, so that the total length (measure) of the Cantor set is $(2/3)^n$. This result is characteristic of a fractal set: as $n \to \infty$, the number of details (segments here) grows exponentially to infinity while total mass goes to zero, also exponentially fast. The topological dimension of the Cantor set is $D_T = 0$ since its total length is zero. Hence, the notion of dimension is not very useful as it does not distinguish between this complex Cantor set and a simple point. The simplest dimension that generalizes the topological one is called the capacity dimension:

$$D = \lim_{n \to 0} \frac{\log N_n}{\log(1/l_n)} = \frac{\ln 2}{\ln 3} \approx 0.63.$$

## Fat fractals: synthetic porous media

Fat fractals have been proposed as realistic models of microporous media. The empty holes of fat fractals have size-dependent power distribution similar to porous materials (Umberger & Farmer, 1985; Bulgakov & Konotop, 1992). Compared to thin fractals, the main peculiarity of fat fractals is a finite, non-zero Lebesgue measure of their support, which is the point behind naming them as fat fractals, to distinguish them from thin fractals.

## Construction of fat fractals

Two kinds of fat fractals can be constructed: regular and mixed fat fractals.

## 1. Regular fat fractals

Regular fat fractals can be obtained by iterating a simple rule. Let us recall how a 1D regular fat fractal is generated. For the sake of simplicity, we usually deploy the unit interval as initiator. A regular fat fractal can be obtained through the following simple iterative rule: from one step to the next, we just drop the open middle intervals of length $l_n$ from each of the remaining intervals. If the length of the interval at step n-1 is $L_{n-1}$, then this removed length is $L_{n-1}$ divided by $a^n$. After n iterations, the obtained set is composed of $2^n$ intervals of lengths $L_n$ and n subsets which are composed of $N_{n(k)}=2^{k-1}$ empty holes of lengths $l_k$, k=1,2,..., n, respectively. For a 1D regular fat fractal, a is the only parameter involved in its definition. The first 4 iterations of a regular fat fractal are depicted in Figure 1.3.



**Figure 1.3: A regular fat fractal with $a$=2**

It is clear that the empty holes of a regular 1D fat fractal are symmetrically distributed in 1D. To describe a porous medium having asymmetric features, we have to use mixed fat fractals.

## 2. Mixed fat fractals

Intuitively, a mixed fat fractal is the redistribution of parts of the regular one, obtained by rearranging its voids and occupied intervals alternatively. By changing the distribution of the empty parts of the regular fat fractal in a random way while respecting the number of segments, their size and, finally, segment-hole-segment order, a mixed fat fractal will be created.



**Figure 1.4: A mixed fat fractal obtained from the regular one represented at the bottom of the image,**

$a=4$

It is noteworthy that the random distribution of holes offers a huge number of possibilities to construct a mixed fat fractal from the same regular one. More precisely, the possible number of mixed fractals $NP(n)$ after n iterations can be expressed by (Li et al., 2004; Nekka et al., 2005):

$$NP(n) = \frac{(2^n - 1)!}{(2^{n-1})!} \times NP(n-1) \qquad \text{With} \qquad NP(1) = 1$$

For example, when $n = 4$, the possible number of mixed fat fractals would be about $NP(4) = 20,432,412,000$. We must also mention that fat fractals have been processed by more sophisticated tools (Nekka et al., 2005) combining the ACF and the regularization dimension, a method proposed to estimate curve variation. Indeed, the spectral analysis

that we use in this thesis is not appropriate when complexity increases, as is the case with fat fractals.

In fact, Nekka and Li ( Nekka & Li, 2004) proposed to use of the regularization dimension to quantify variations exhibited by the autocorrelation function of these structures. Comparison of the obtained results shows that, when the regularization dimension is directly applied to the structures, a differentiation based on this dimension is less convincing compared to when it is applied to their autocorrelation function. In fact, the regularization dimension of the autocorrelation function has been shown to be a strictly increasing function of the size of the initial hole of the fat fractal. This difference can be explained by the fact that autocorrelation function has a smoothing "action" since it attenuates the irregularities of a signal (spatial signal representing the set in this case) and produces more uniform ones: sparse parts intersecting with themselves will still be sparse and when intersecting with denser parts, will again produce sparse parts ( Nekka & Li, 2004). Also, the autocorrelation accumulates similarities that are dispersed all along the set. Once the autocorrelation function is applied, the similarity amount is globally decreasing as the translation value t increases.

## Lacunarity

The concept of lacunarity was coined by Mandelbrot to refer to gap distribution in a fractal. Over the years, lacunarity has been taken into account as a distinguishing factor between sets of the same fractal dimension (Smith et al., 1996). As formulated, lacunarity is a scale-dependent measure of spatial heterogeneity of a complex texture. It gives a value of "gappiness" of a geometric structure. Low lacunarity indicates the homogeneity of the set because all gap sizes are similar, while high lacunarity implies that the set is heterogeneous and consists of a wide range of gap sizes.

Methods for calculating lacunarity were first developed in general terms by Mandelbrot (1982). A theoretically and computationally simple way of calculating lacunarity is the "gliding box" algorithm (Allain & Cloitre, 1991). With this method, which derives from the box-counting technique, the square box of given length $a$ is first placed at one corner of a set, for example, a binary image with 1 and 0, which are defined

as occupied and unoccupied regions, respectively. Therefore, the images must be thresholded prior to analysis. Then, the number of occupied pixels or box mass, having the value of (1), is determined. The box is thoroughly going through the image at 1 pixel (cell) at a time, and $S$, the number of occupied sites, is determined for each of these overlapping boxes.

Lacunarity $(L_{la})$ for box size $a$ is obtained by the ratio of variance of the number of occupied sites to the square of the mean number of occupied sites plus 1:

$$L_{la} = 1 + \text{var}(S) / E^2(S)$$

where $E(S)$ is the mean and $var(S)$ is the variance of the box mass values for box size $a$. Spatial heterogeneity can be quantified by means of a lacunarity curve, a log-log plot of lacunarity against box size $a$, at different scales. Furthermore, lacunarity is obviously a function of 3 variables, size of the gliding box, fraction of the map occupied by the object of interest, and the geometry of the map, as measured by a gliding box approach. Lacunarity is not related to fractal dimension $D$, but strongly interacts with the size distribution of holes on the texture and with its deviation from translational invariance. One of the main criticisms of this method is the shifting from one box size to the next size, which creates huge jumps and consequently-scattered data. Therefore, despite its popularity, the method still suffers from being degenerate in rather simple cases where 2 deterministic regular shapes of the same fractal dimension cannot be resolved (Nekka & Li., 2003b). More advanced methods have been developed recently. The Hausdorff measure function spectrum is one of them (Nekka et al., 2005).

## The Hausdorff measure function spectrum (HMFS)

Since structures can have different degrees of complexity, various strategies have to be adopted to find suitable tools for the extraction of information with the least degeneracy dimension (Nekka et al., 2005). First, for the porous media studied in this thesis, we have developed an appropriate method based on the ACF that we exploited to

extract complementary parameters beyond porosity, using spectral analysis. For the fractal-like structures mentioned above, with intermediate complexity and integer dimension, the combination of autocorrelation with the regularization dimension led to a more robust classification (Li et al., 2004; Nekka et al., 2005). Thin fractals have non-integer dimensions and high complexity. For this kind of complexity, I will briefly explain how, in their work, Nekka and Li (2004) have proposed a new method called the HMFS as an original means to give complementary characteristic parameters beyond fractal dimension.

First, let us recall the motivation for developing the HMFS method. Considering fractal dimension as a first-degree complexity, the HMFS has been designed to distinguish 2 different structures having the same fractal dimension and to estimate their degree of homogeneity as well. Typical non-trivial examples are sets having zero-Lebesgue measures, as is the case for Cantor sets, or, more generally, thin fractals. The HMFS involves integration according to Hausdorff measure $H^s$ instead of the Lebesgue measure used in the ACF. In fact, the HMFS is defined as follows (Li et al., 2004; Nekka et al., 2005):

$$I^{SH}(t) = \int_{x \in F} \chi_F(x)\chi_F(x+t)dH^{SH}(x)$$

The HMFS is based on the combination of 2 concepts: the autocorrelation function and the Hausdorff measure. The former indicates the similarity of the sample's distribution, while the latter is dedicated to complexity quantification. This explains why the method gives a more complete description of the geometric structure of sets and distinguishes between sets having the same fractal dimension (Li et al., 2004; Nekka et.al., 2005).

In the following pages, we will also recall the Fourier transform (FT), since we use it as a practical tool to complement the method we developed.

## The Fourier transform (FT)

Fourier theory, introduced by Jean Baptise Fourier (1768-1830), is widely employed in many fields, such as engineering, physics, applied mathematics, and chemistry. The FT is an appropriate tool to handle problems associated with signal processing and analysis. In fact, the FT breaks down a signal into its constituent parts by identifying different sinusoidal frequencies and their related amplitudes.

It is common to write the FT $X(f)$ formula of continuous signal x (t), and its inverse, as follows:

$$X(f) = \int_{-\infty}^{\infty} x(t).e^{-j2\pi ft} \, dt$$

$$x(t) = \int_{-\infty}^{\infty} X(f).e^{j2\pi ft} \, df$$

The FT of the periodic signal can be presented by the following pair:

$$X(kf_0) = \frac{1}{T_0} \int_{0}^{T_0} x(t).e^{-2\pi kf_0 t} \, dt$$

$$x(t) = \sum_{k=-\infty}^{\infty} X(kf_0).e^{j2\pi kf_0 t}$$

where frequency $f_0$ of the periodic sample is:

$$f_0 = \frac{1}{T_0}$$

## The discrete Fourier transform (DFT)

Continuous (analogue) signals have to be sampled when deployed in computerized methods. This is done by applying a sampling frequency that is called the *Nyquist frequency*. The amount of this frequency has to be at least twice the maximum frequency in the continuous signal. The sampling process is performed by recording (sampling) the value of the continuous signal at regular points to get a sequence of numbers.

Now, if we assume that signal *x(t)* is sampled N times per period of *T* seconds, the DFT and its inverse, for a periodic or a complex valued series, are written (Partt, 2002) as:

$$X(k) = \sum_{n=1}^{N} x(n) \cdot e^{-j2\pi(k-1)\left(\frac{n-1}{N}\right)}, \ 1 \le k \le N$$

where $N$ is the total number of samples, and $k$ is the spectral domain index. The DFT equation shows that for a N sample sequence, such as a 16-bit sample, 16 output samples are produced in the frequency domain. However, because of the Twiddle factor, we only need the first half of the samples. In Figure 1.5, we illustrate some typical harmonic signals and their corresponding DFTs to gain a better understanding of the relationship between these signals and their DFT spectrum (Bourke, 1993). It is obvious that for the constant signal shown at the top right of Figure 1.5, there could be no frequency impulse as depicted in its related DFT spectrum shown on the top left. For the signal representing the first harmonic at the middle left of Figure 1.5, we got one frequency impulse at the frequency of the sine wave. The DFT signal was shifted to 2 for the second harmonic.

The DFT equation involves $N^2$ arithmetic operations (additions and multiplications) which can be too large. In fact, the number of computations is manageable for small samples, whereas the calculation can scale up to unmanageable proportions as the number of samples increases (Bracewell, 1965).
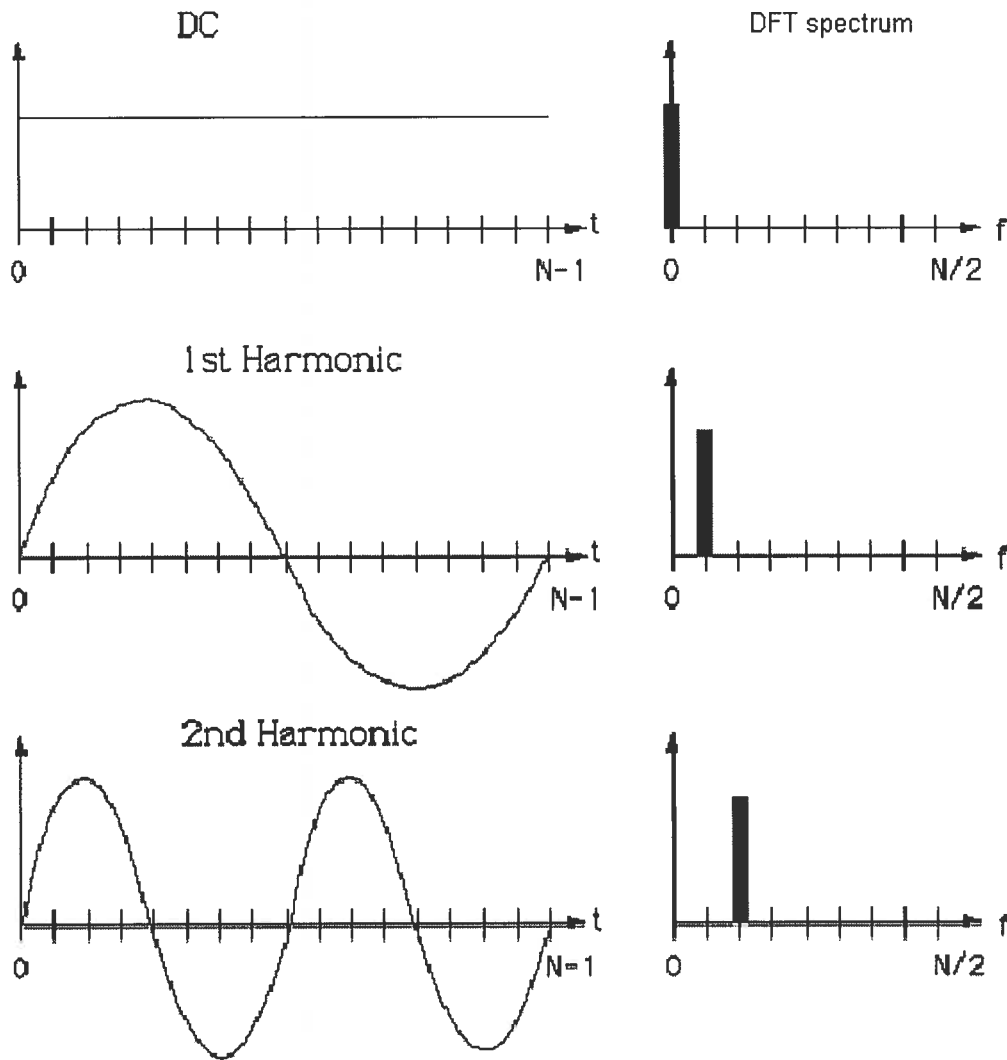
**Figure 1.5: Illustration of harmonic signals and their related DFT components**

## The fast Fourier transform (FFT)

The FFT was proposed by Cooley and Tukey in 1965. The idea behind the FFT is to decompose the DFT operation into a number of other DFTs with shorter lengths and to achieve much faster computation for the large values of sample N. Therefore, the FFT offers another method of achieving the same results with less calculation. The FFT breaks up the original $N$ point sample into 2 *(N/2)* sequences, and, consequently, the FFT algorithm reduces the number of operations to approximately $N.log_2N$.

However, it is more convenient to estimate the FT with the DFT rather than the FFT algorithm readily implemented in available software. The reason for this choice is that we are more concerned here with accuracy rather than with processing speed. Indeed, the range of frequency values for the textures we analyze in this work was not large enough to necessitate a rapid process. However, the frequency values were close enough, making it necessary to employ the DFT variant to obtain good accuracy and to differentiate between textures.

## Porosity and the autocorrelation function (ACF)

In this project, the autocorrelation function and the Fourier transform of images exhibiting periodic patterns are investigated to provide a quantitative geometric characterization of porous structures. In fact, we revisit the autocorrelation function and propose an original way to reveal the morphology of porous media beyond porosity. We use typical thread-like structures to show how our newly-developed analytical approach allows the extraction of pore frequency and extent, which are parameters complementary to porosity.

## Objectives

The objectives of the current work are to:

- Reveal the morphology of porous media by means of the decomposition of bi-phase images under the action of 2 types of methods, the autocorrelation function and the discrete Fourier transform.

- Develop additional parameters to quantify details of heterogeneous textures beyond porosity.

In this thesis, we address the fundamental problem of quantifying texture and the continuous need to develop a more precise tool, by devoting the entire first chapter, *Introduction*, to the challenge in various approaches and material characterization techniques, focusing particularly on polymeric porous media. The second chapter consists of 2 parts. The first part explains basic theory behind the *Methodology*, the autocorrelation function and the FT methods. Emphasis is placed on the way these methods are applied for analysis. In the second part, *Applications*, the applied, modified analyses and results are followed by a full discussion. Whenever possible, practical algorithms are described and illustrated in detail.

In fact, we validate this approach with examples and its applicability is demonstrated by various cases such as:

Case 1: Same porosity and different DFT values

Case 2: Same DFT but different porosities

We also apply this analysis to porous polymeric images to underpin the idea that the obtained parameters stay independent of the chosen threshold during binary image processing. Finally, in the third chapter, *Conclusion*, we summarize the results of the present work and cite some perspectives.

# CHAPTER 2: METHODOLOGY AND APPLICATIONS

## Methodology

In the present work, two kinds of porous images, polymeric porous media and synthetic thread-like textures, are taken to illustrate the method and the different steps involved. They are also immediate applications of the strategy developed.

## Correlation and autocorrelation functions

The correlation process is a powerful tool to measure the similarity between 2 signals as a function of shift amount $t$ between them. It has been traditionally used to characterize the properties of irregular functions (Champeney, 1973). We must recall the mathematical formulation of the correlation function (CF) between 2 signals, $f$ and $g$:

$$y(t) = f * g = \int_{-\infty}^{\infty} f(x)g(t+x)dx \qquad Eq.1$$

To clarify this concept graphically, Figure 2.1.b illustrates a signal g shifted with respect to another signal f in Figure 2.1.a. The result of multiplication of each element of the 2 signals at shift point $t$ is shown in Figure 2.1.d. Thus, integration based on Eq. 1 over all $t$ values to find the area under the product gives the value of the CF (Figure 2.1.e).

The following figure depicts the autocorrelation process between signals f and g.
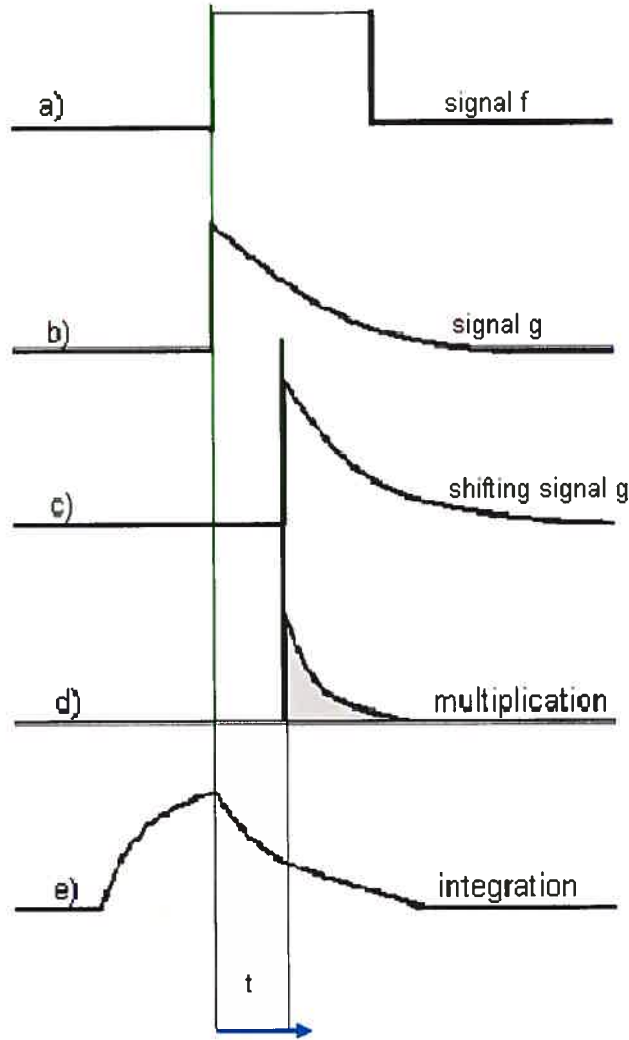
Figure 2.1: Illustration of the correlation function of 2 signals

The process of the CF, as illustrated in Figure 2.2, highlights 3 main properties which are exploited in our analysis. First, the largest value of positive correlation in this diagram is obtained when 2 signals are thoroughly similar in shape or phase. As one signal is shifted with respect to the other, the signals go out of phase, so the correlation gets smaller and the peak shows negative parts. The breadth of the significant value of the CF peak reveals how long the signals remain similar, in other words, it expresses the width of the same phase in the texture.
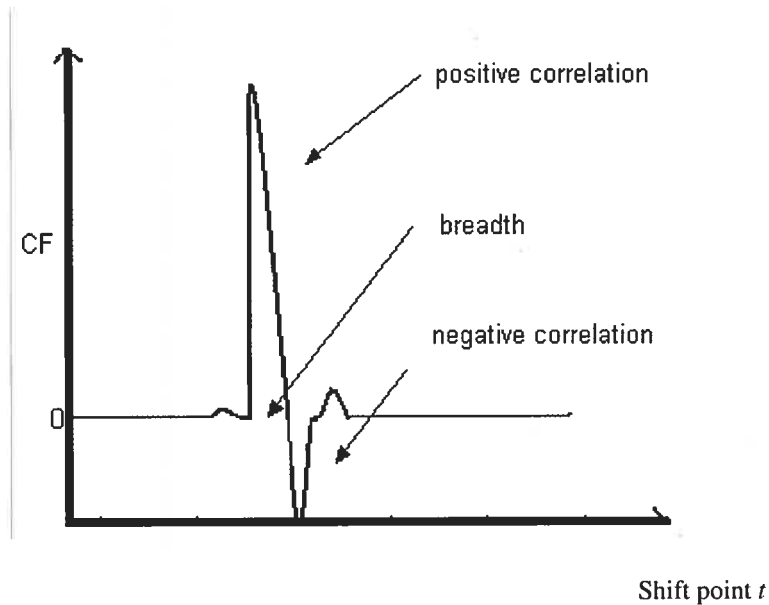
Figure 2.2: Illustration of correlation properties

The autocorrelation function is a particular case of the correlation process since correlation of the signal with itself is investigated. In other terms, when f(x) and g(x) are the same, the term autocorrelation function is used rather than the correlation function. The involved translation operation provides a sieving action which seems to be the best way to accumulate and reveal the most significant geometric structure of the set, expressed through its similarities (Li et al., 2004). Indeed, this self-crossing process sums all point-point similarities (by product) of the signal at distance t.

The mathematical definition of the autocorrelation function is thus:

$$y(t) = f * f = \int_{-\infty}^{\infty} f(t+x)f(x)dx \quad Eq.2$$

# Image characterization using the autocorrelation function

Correlation has been used successfully in time series to quantify similarities between 2 functions. It has been applied to mass spectra of polymers such as the silsesquioxane-siloxane copolymer (Wallace & Guttman, 2002). However, the reader will see how we revisit it in this work for a spatial signal to propose an original way of gaining insight into structures.

## Porosity and the autocorrelation function: a new approach

Porosity is a dominant pore structure measure of porous media. Porosity refers to occupancy of the set, measured on samples having regular geometric shapes. Hence, porosity indicates how dense porous media is when considered in the space where it lives (Nekka & Li, 2004). We show here how we can recover porosity from the autocorrelation function. This connection is not meant in a deterministic sense (for 1 sample), but rather in a statistical way.

## Porosity and the autocorrelation function: the algorithm

In this work, we take a new analytical approach to revisit the autocorrelation function to extract 2 independent components, which we relate to porosity as well as to pore frequency and extent. In a first step, we will practically prove how to extract image porosity by the least mean square (LMS) slope of the autocorrelation function. In a second step, we will subtract the LMS slope from the autocorrelation function to keep the information hidden in the oscillating part, thus excluding porosity. Finally, we apply the FT on this remaining oscillating curve to obtain the main frequency components.

Let us summarize the 3 steps of the method:

**1)** Calculation of the autocorrelation function, starting from the matrix of the input image.

**2)** Estimation of the slope of the autocorrelation function by the LMS and subtraction of this LMS slope from the autocorrelation function curve.

**3)** Calculation of the FT of the remaining part of the.

We will go into more detail with these steps.

## 1) Calculation of the autocorrelation function starting from the matrix of the input image

Since we are only concerned with geometric structures, we rewrite the particular case of the autocorrelation function, where f in Eq. 2 above is reduced to the indicator function $\chi_F(x)$ of the structure. We denote this particular case of the autocorrelation function for the indicator function by $I$, that is:

$$\boxed{I(t) = \int_{x \in F} \chi_F(x) \cdot \chi_F(x+t)dx}$$

where F refers to the image, i.e. image information represented by (black) pixels, and $\chi_F$ is the indicator function of F:

$$\begin{cases} \chi_F(x) = 1 \text{ si } x \in F \\ \chi_F(x) = 0 \text{ si } x \notin F \end{cases}$$

The algorithm has been implemented with Matlab® software. Two important facts have to be mentioned when applying the above definition:

- The application field is spatial rather than temporal.
- The discrete version has to be implemented rather than the continuous one since we are dealing with image pixels.

Matlab® software automatically transforms the input sample films into a binary image over a given threshold. First, the grey level image is converted into a matrix (with the Matlab command *imread*). The image is then binarized with a threshold value which is an integer number between 0 and 255. Matrix elements below this threshold are set to 0 (black), and those which are larger are set to 255 (white). Thus, the binarized image is darker when the threshold value is large, and inversely.

Let A be the image matrix. Then, the following algorithm is applied:

Let $A = (a_{i,j})$ a $n \times m$ matrix.

Let $C(i)$ be the ith component of the autocorrelation vector that has to be calculated. We have:

$$C(i) = \frac{\sum \sum b_{j,k}}{\sum \sum a_{j,k}}$$

where the matrix $B = (b_{j,k})$ is obtained by multiplying, term by term, 2 matrices, truncated from A, one is formed by columns i to m of A, and the other is formed by columns 1 to m-i+1 of A. Hence, vector C contains m components.

The method (translation) is used in the horizontal direction of the image on a collection of parallel 1-D samples. The similarities to be detected have thus to be present in the translation direction. The mean of the autocorrelation function of these samples is then estimated to represent the whole image.

## 2) Estimation of the slope of the autocorrelation function by the LMS and subtraction of this LMS slope from the autocorrelation function curve

Let us illustrate this second step by a practical example. First, we will practically prove how to extract image porosity with the LMS slope of the autocorrelation function. Then, we will subtract this LMS slope from the autocorrelation function to keep the information hidden in the oscillating part, thus excluding porosity. To explain our procedure, we deploy a set of porous images of decreasing porosities, representing polymeric porous structures taken from Kai et al. (2003). These blending films of porous scaffolds are obtained by scanning electron micrography (SEM). The decreasing porosities are dependent on the concentration of the 2 polymers used, poly-

(hydroxybutyrate-co-hydroxyhexanoate) (PHBHHx) and poly-hydroxybutyrate (PHB) (Figure 2.3). Figure 2.4 reports the equivalence (matching) between the LMS slope of the autocorrelation function of Figure 2.3 (a-f) and the porosity values calculated by the porosity formula.
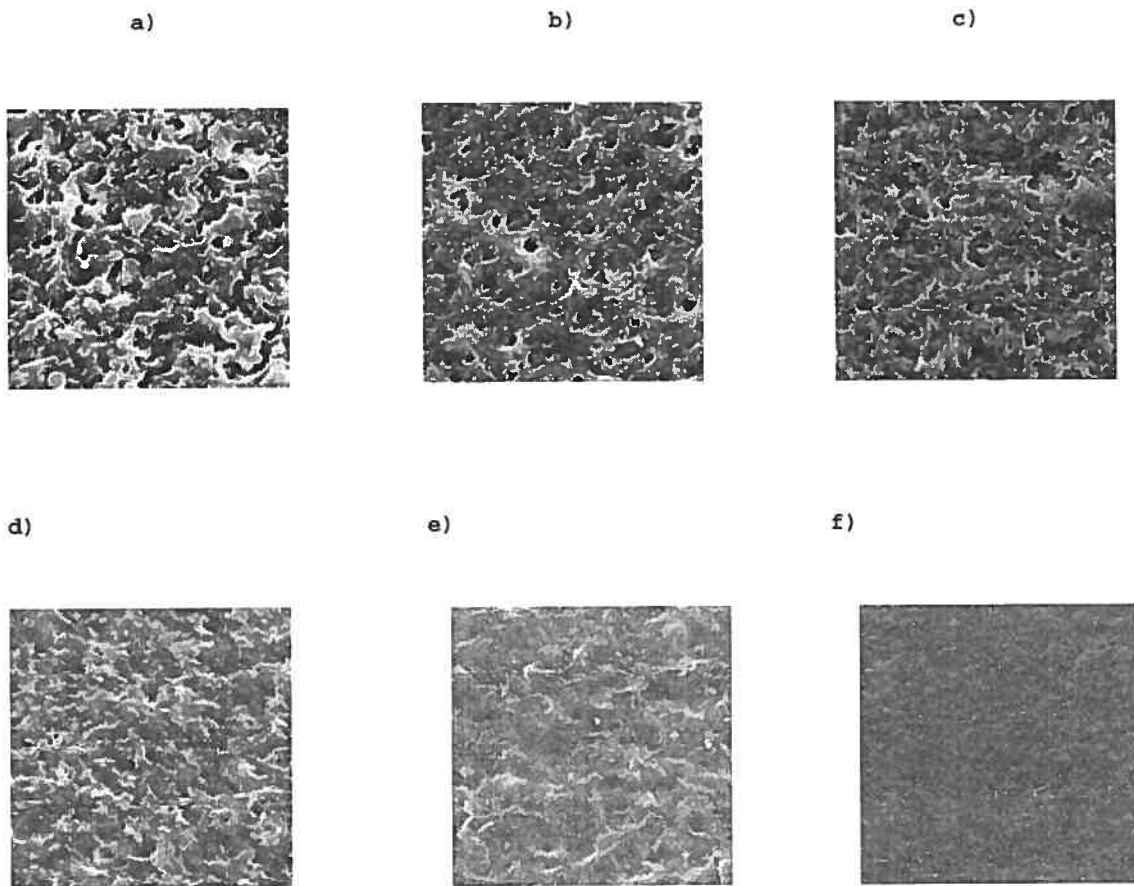
a)

b)

c)

d)

e)

f)

**Figure 2.3. Scanning electron micrograph of surface morphologies of PHBHHx/PHB blending films with various ratios of PHBHHx/PHB: (a) PHB; (b) PHB80/PHBHHx20; (c) PHB60/PHBHHx40; (d) PHB40/PHBHHx60; (e) PHB20/PHBHHx80; and (f) PHBHHx.**
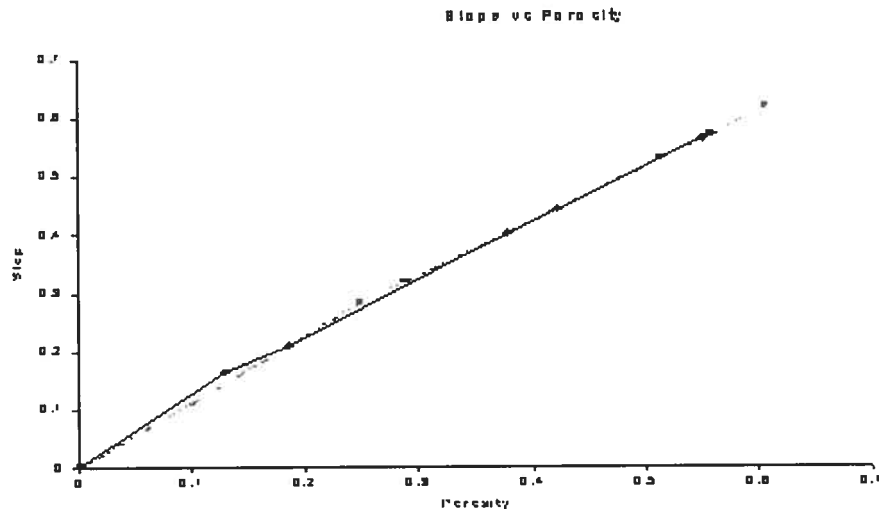
**Figure 2.4: Matching between estimated porosity and the LMS slope of the autocorrelation function**

## 3) Calculation of the FT of the remaining part of the autocorrelation function

Now, we need to analyze the remaining oscillating curves of which porosity information has been cleared, to extract complementary parameters for periodic patterns. To do this, we take the case of 2 different thread-like patterns shown in Figure 2.5, both having the same porosity value of 0.4633. When the porosity value is dropped, we apply the FT to the oscillating curve. The result is shown in Figure 2.6. For the thread-like textures that we synthesized, it is more convenient to estimate the FT with the DFT as mentioned above. The DFT is more accurate than the FFT when the analyzed frequencies are low. Indeed, the FFT is of great use for huge frequencies, and its main advantage corresponds to the fast speed of the process, while the DFT is slower to calculate but provides better precision (i.e. with better resolution) for close frequencies.

In our study, the frequencies were close enough, making it necessary to employ the DFT variant to obtain good accuracy to textures. The results on frequency f as well as

on 1/f give 2 parameters independent from porosity, representing the number of strips as well as their size, respectively.

Figure 2.5 (a and b) shows 2 bi-phase structures containing 2 and 9 black strips. We have constructed these binary synthetic porous structures of periodic black and white strips that we called thread-like textures, with values of either 0 (void phase) or 1 (matrix phase). These thread-like textures, which present regular and ordered microstructures, are of equal size of [140 × 140] pixels, and stored as bmp type files. Hence, black zones represent the unoccupied area of the image and are associated with pores in the image. In contrast, the white zones show occupied areas. As seen in Table 1, both images have the same amount of porosity, equal to 0.4633. For each image, the autocorrelation function and its DFT are given in Figures 2.6 and 2.7, respectively.
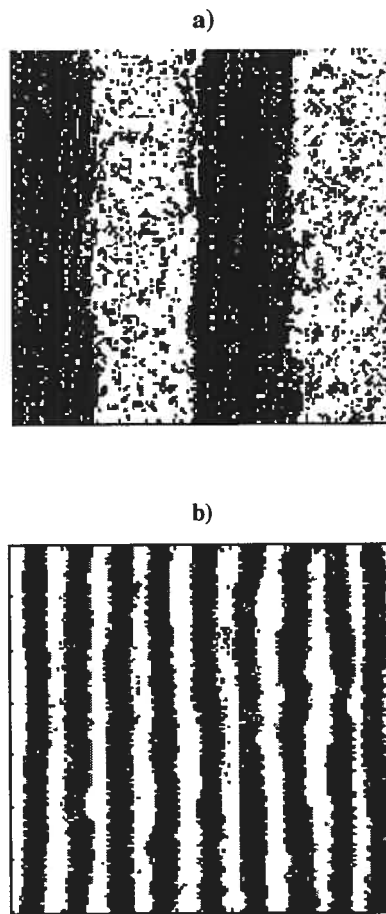


**Figure 2.5: Bi-phase porous media of thread-like textures with the same porosity but different main frequencies**
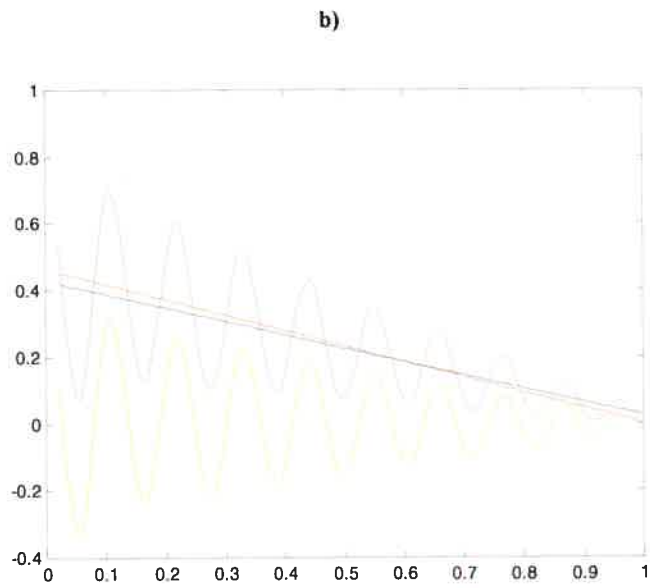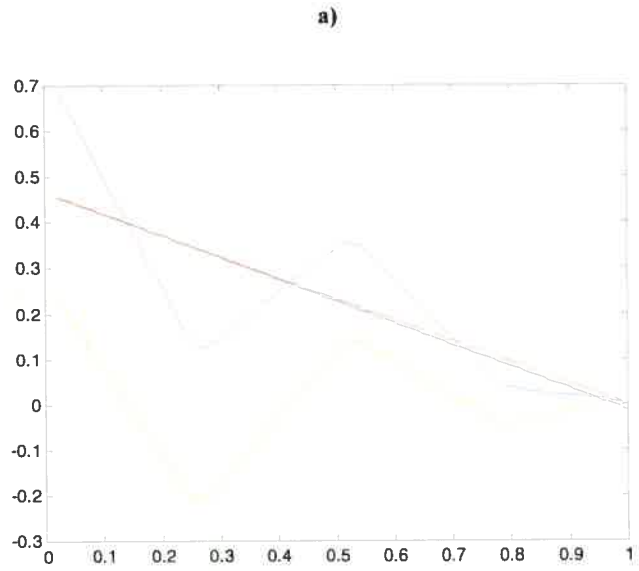
**Figure 2.6: Autocorrelation spectrum of (a) Figure 2.5.a, and (b) Figure 2.5.b**
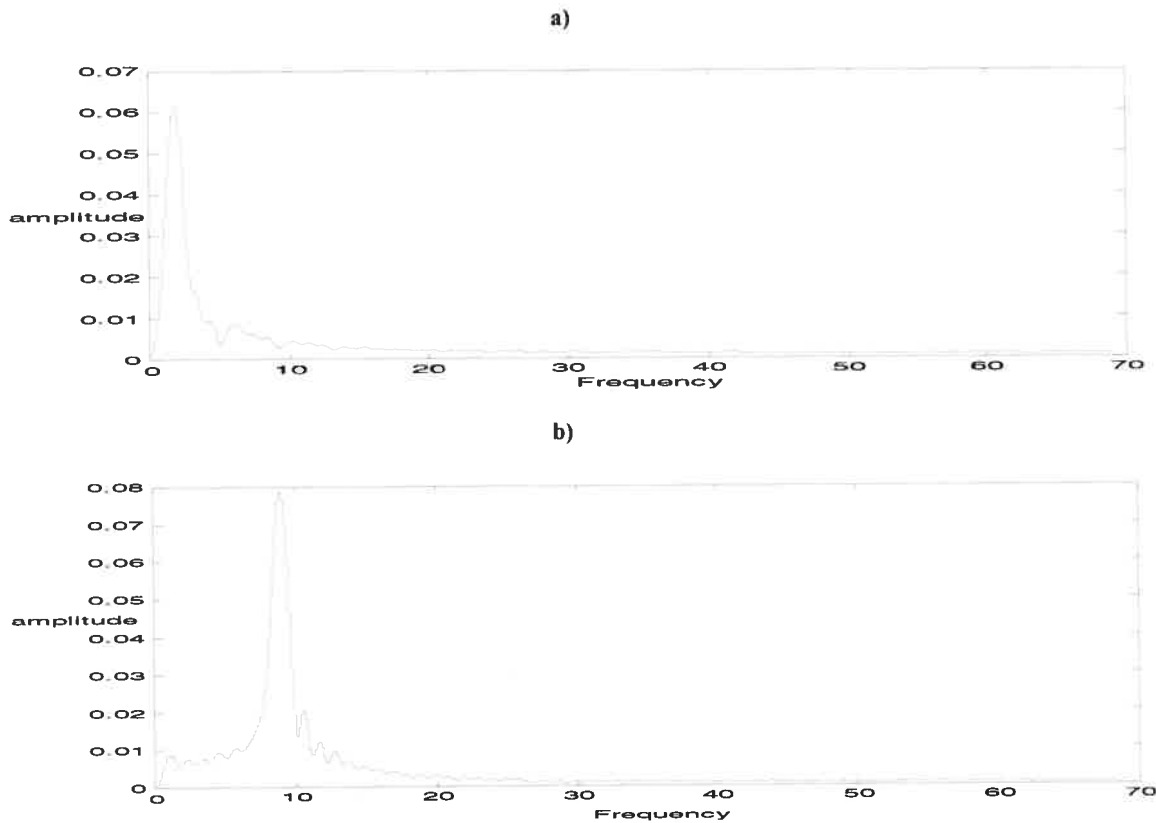
**Figure 2.7: The DFT spectrum of (a) Figure 2.6.a, and (b) Figure 2.6.b**

|  | Porosity | $f$ | $1/f$ |
|---|---|---|---|
| **Figure 2.5.a** | 0.4633 | 1.83 | 0.55 |
| **Figure 2.5.b** | 0.4633 | 8.99 | 0.11 |

**Table 1: Porosity and DFT frequency of Figure 2.5**

In general, the FT plot reveals a certain number of frequencies from high to very low amplitudes. Here, only one frequency appears with large amplitude. This frequency corresponds to an element of the image presenting similarities through the structure. Thus, analysis with autocorrelation, on this kind of periodic images, emphasizes the

repeated feature embedded in the image, namely, the elements of the thread, making it possible to also determine the frequency with which these elements are present in the image.

We thus obtain from the autocorrelation function analysis the following 2 parameters:

1. Porosity
2. Thread number per unit length.
The main characteristic of these 2 parameters is their independency.
To the best of our knowledge, it is the first time that this kind of processing has been performed on the autocorrelation function representing a geometric structure.

## Applications
## Results and Discussion

Now that the method has been explained and illustrated in the above examples, we will go into some further details. We again use the films of porous PHBHHx/PHB scaffolds presented in Figure 2.3. We recall that these electron micrographs of size equal of [140 × 140] pixels, have decreasing porosity as the PHB concentration declines until a free pore surface is obtained with the pure PHBHHx scaffold. We estimated porosity at a fixed threshold value (here at 127 as a mean value of the whole threshold) and compared it with the slope of the autocorrelation function. Figure 2.8 illustrates the obtained binary image from Figure 2.3 a. as an example
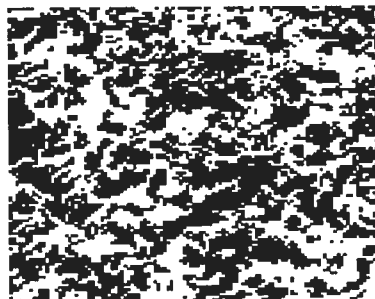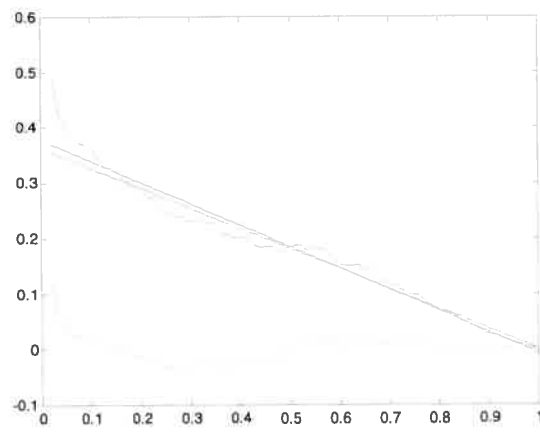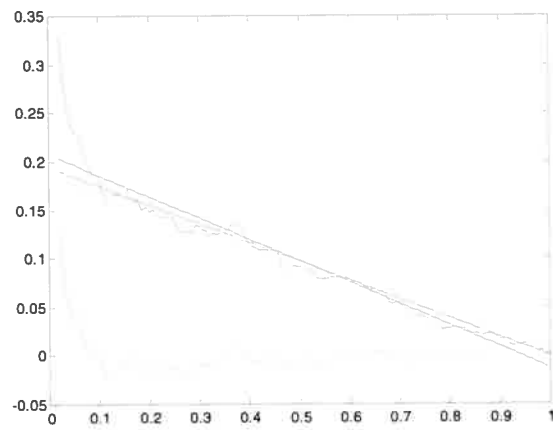


**Figure 2.8: An example of binarization with threshold 127 of Figure 2.3.a**
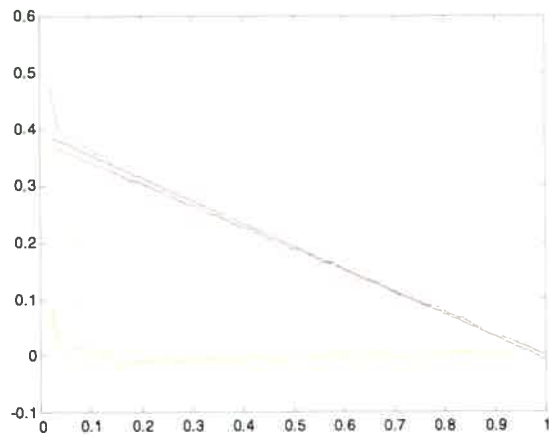
a) The autocorrelation function spectrum of Figure 2.3.a



b) The autocorrelation function spectrum of Figure 2.3.b

**c) The autocorrelation function spectrum of Figure 2.3.c**
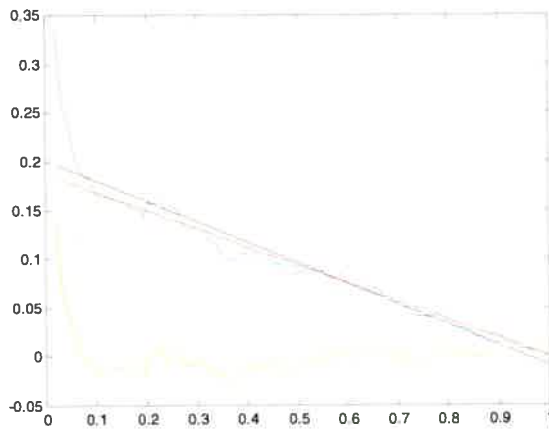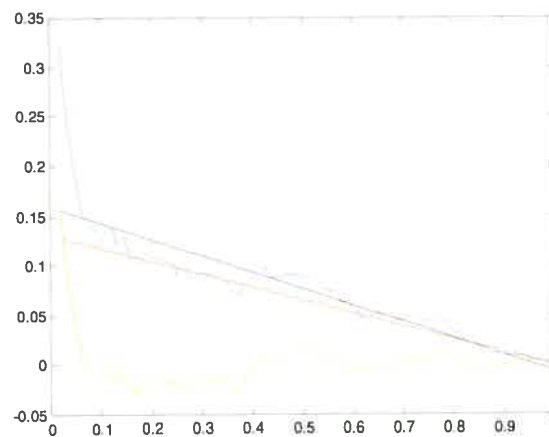


**d) The autocorrelation function spectrum of Figure 2.3.d**



**e) The autocorrelation function spectrum of Figure 2.3.e**

f) The autocorrelation function spectrum of Figure 2.3.f
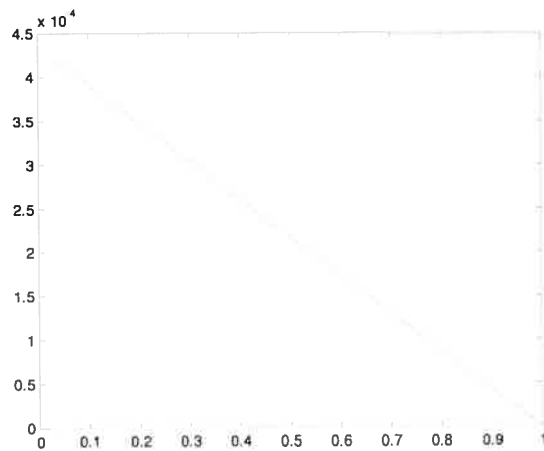


**Figure 2.9: Illustrating the details of the applied autocorrelation function on each image of Figure 2.3**

The different components of the autocorrelation function spectrum in Figure 2.9 are illustrated in different colors. Blue represents the autocorrelation function; red corresponds to the linear part of the spectrum; black is the slope of the spectrum obtained by the LMS; and, finally, green shows the spectrum after dropping the linear part. The porosity of these textures along with the calculated slopes of the autocorrelation function is listed in Table 2.

|  | Slope | Porosity | $\alpha$ |
|---|---|---|---|
| **Figure 2.3.a** | -0.5647 | 0.5514 | -1.02 |
| **Figure 2.3.b** | -0.4437 | 0.4229 | -1.04 |
| **Figure 2.3.c** | -0.4014 | 0.3779 | -1.06 |
| **Figure 2.3.d** | -0.2107 | 0.1866 | -1.13 |
| **Figure 2.3.e** | -0.1656 | 0.1304 | -1.27 |
| **Figure 2.3.f** | 0 | 0.0004 | 1.00 |

**Table 2: Slope and porosity of Figure 2.3**

These results show that no significant differences exist between the slopes of the autocorrelation function and calculated porosity. In fact, it is reasonable to consider that these 2 parameters (slope and porosity) are related in a linear manner with a constant $\alpha$ close to 1:

$$slope \cong \alpha \ porosity$$

At this stage, we have to mention that a rigorous proof of this relationship has been given by Nekka and Li on some typical examples of porous media such as single component and double component media with point-to-point independence as well as single component of porous media with correlation between points in terms of their distances (Nekka & Li 2005).

## Oscillations of the autocorrelation function spectrum

To study the remaining oscillations of the curve spectrum, several cases of synthetic as well as real porous images will be employed. Of course, it will be of no interest if porosity was the only parameter extracted from the autocorrelation function. The idea is to find an independent parameter from porosity to additionally characterize porous media. Since we proved that the linear part of the autocorrelation function is really image porosity, there was no need to keep this information within the signal. Hence, we withdraw the linear part from the autocorrelation function spectrum so that only the oscillations are kept. To this oscillation curve, the DFT has then been applied to extract the information included. We want to emphasize that, without eliminating the linear part of the autocorrelation function (the LMS slope), information about significant frequency will be tangled up in redundant data, because of the inclusion of FT of this linear part.

To begin, let us highlight the need for this additional and independent information, by analyzing the case of images having the same porosity but different structural organizations. The structure shown in Figure 2.5 is such an example.

**Case 1:** **Same porosity and different DFT values**

Recall that Figure 2.5 represents bi-phase structures containing 2 and 9 black strips. As already mentioned, black and white areas are defined as unoccupied and occupied regions, respectively. Both images, as shown in Table 1, have the same amount of porosity, $\phi$ = 0.4633. For each image, the autocorrelation function and its DFT have been given in Figures 2.6 and 2.7, respectively.

From the DFT spectrum in Figure 2.7, we retain the main peak. This peak refers to main frequency $f$ (in terms of its amplitude), which identifies the predominant periodic function exhibited by the autocorrelation function signal. The main frequency is representative of the number of black strips. The results closely correlate with the details included in the images. Indeed, the results indicate a frequency of $f=2$ for Figure 2.5.a, which corresponds to the 2 strips included in this figure, while a frequency of $f=9$ for Figure 2.5.b corresponds to its 9 strips.

The inverse of main frequency $1/f$, shown in Table 2, generally called the period, can be defined as the extent of features in the sample. To obtain the accurate value of the inverse of frequency $1/f$, various resolutions have been used in application of the DFT. Indeed, the $1/f$ of a value of 0.55 for Figure 2.5.a denotes that the extent of the strips in these images is larger than the one in Figure 2.7.b with the value of $1/f$ = 0.11. To illustrate the meaning of these parameters in terms of texture description, we fitted each synthetic texture in Figure 2.5 with its related autocorrelation function and DFT plots as depicted in Figure 2.10. Let us re-emphasize that the DFT is applied to the green curve of the autocorrelation function spectrum.
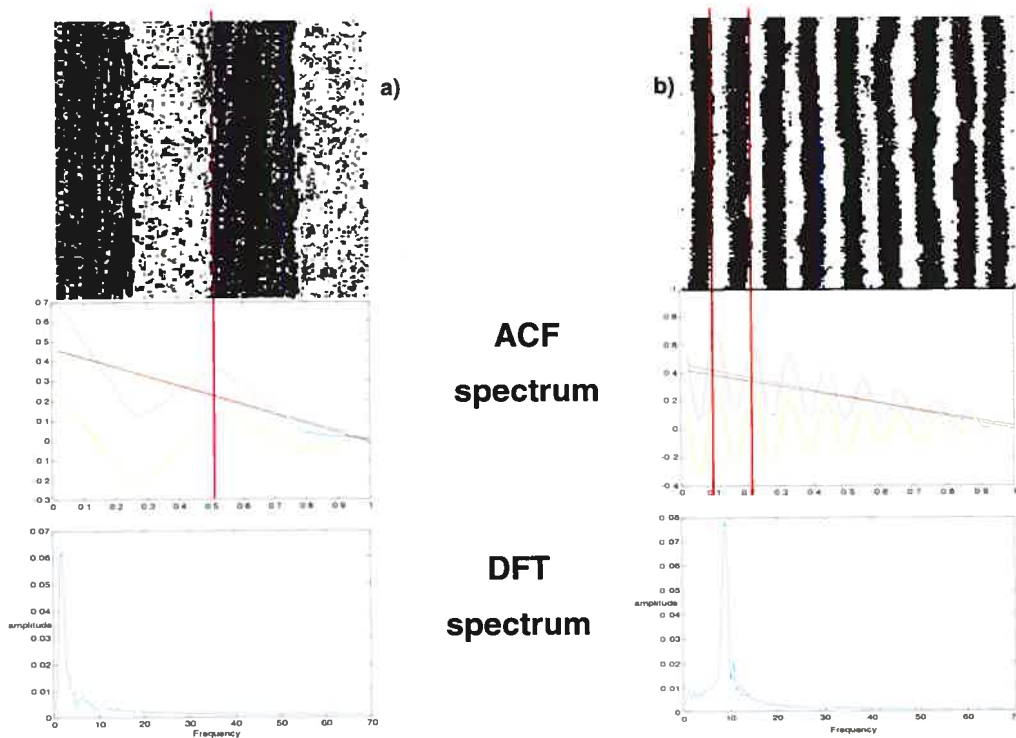
Figure 2.10: Illustration of the meaning of the parameters

## Case 2: Same DFT but different porosities, or why the DFT rather than the FFT?

In this example, we take 2 images having the same FT but different porosities. Figure 2.11 presents 2 porous textures: (a) is a synthetic image containing 3 black-and-white strips, while image (b) is a real texture containing 3 strips. Applying the autocorrelation function to these images gave the spectra shown in Figure 2.12.

Both images display the same main frequency, $f = 3$ in this case, but have different porosities. A resolution of 100 has been used and the obtained 1/f shows the various sizes of the strips for these 2 images, that is, 0.29 and 0.33 for Figures 2.11.a and 2.11.b, respectively. This motivates use of the DFT rather than the FFT since, in this situation, $f$ values are very close. Indeed, in this case, non-integer values of frequency are

required to set structures apart, which is rendered possible by the DFT. Details are given below.
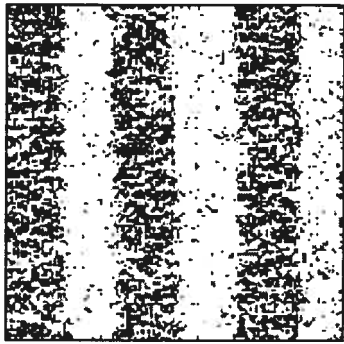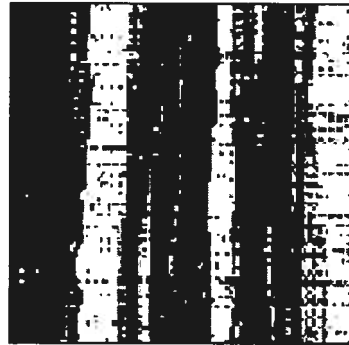


<div align="center">a)                                                  b)</div>

**Figure 2.11: Bi-phase porous media showing the same DFT impulse but different porosities**

a)



b)
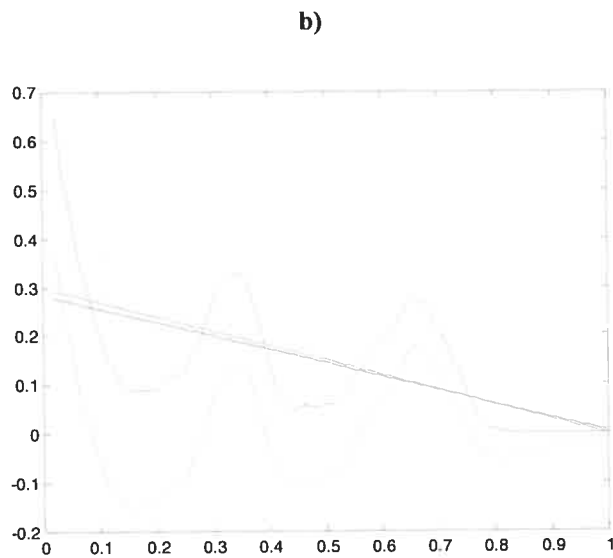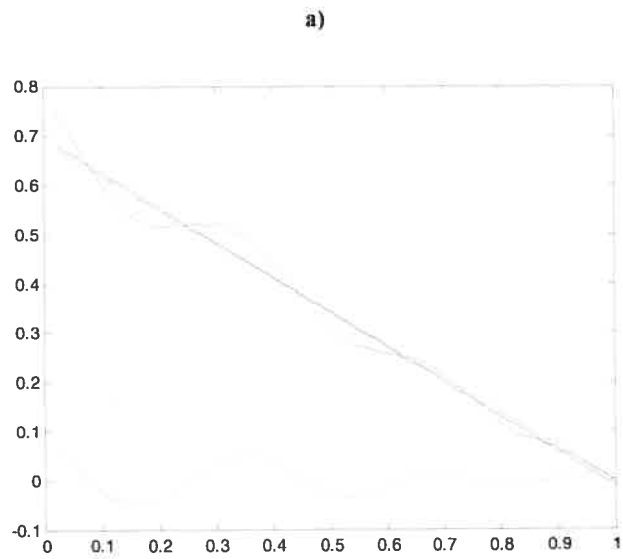


Figure 2.12: The autocorrelation function spectrum of (a) Figure 2.11.a, and (b) Figure 2.11.b

42
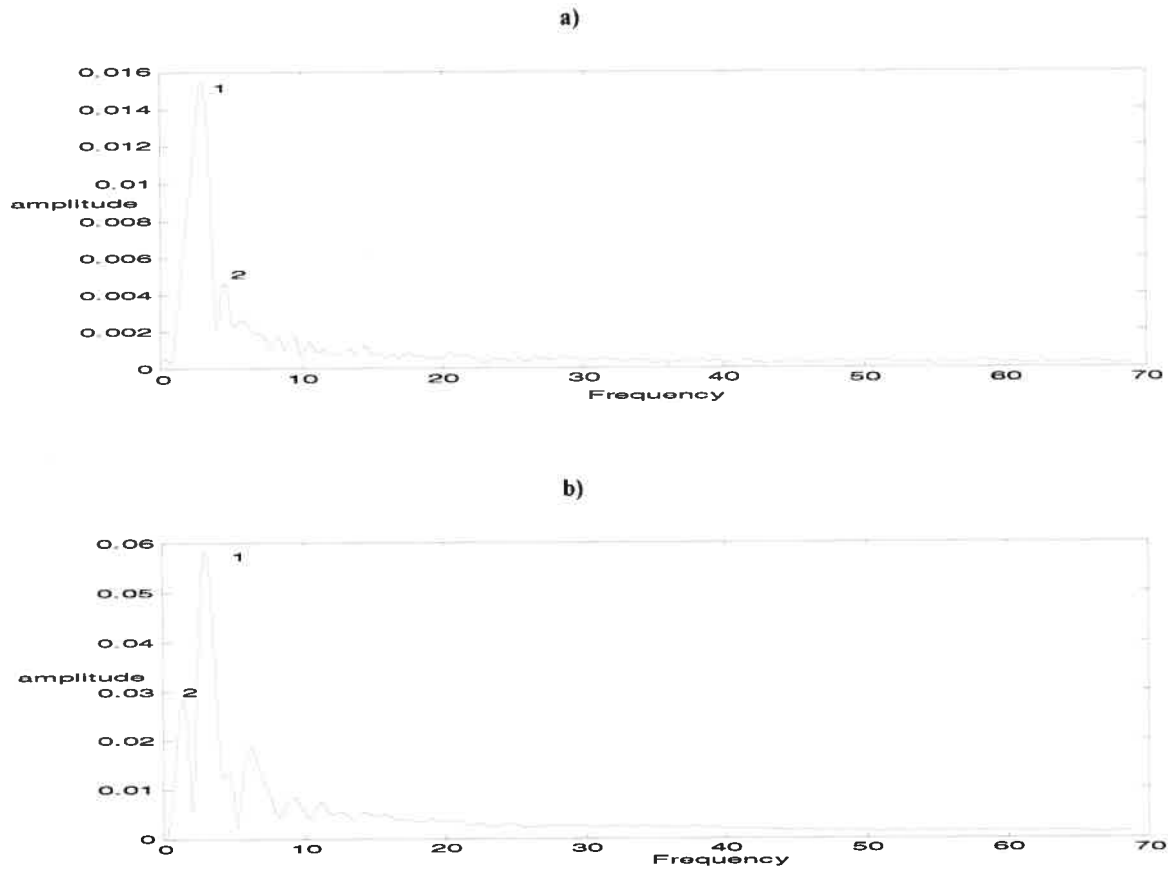
Figure 2.13: The DFT spectrum of (a) Figure 2.12.a, and (b) Figure 2.12.b, using resolution 100

|              | Porosity | f    | 1/f  |
|--------------|----------|------|------|
| **Figure 2.11.a** | 0.3141   | 2.94 | 0.34 |
| **Figure 2.11.b** | 0.7010   | 3.03 | 0.33 |

Table 3: Porosity and DFT frequency of images in Figure 2.11, using resolution 100

Figure 2.13 gives the frequency pattern of the oscillation curves (in green) corresponding to Figure 2.11. We observe the dominance of 1 main peak in the DFT spectrum for both (a) and (b). As seen in Table 3, use of resolution 100 led to the same frequency value, around f=3 for both images. The thread width for Figure 2.11.a is

*1/f*=0.34, and it is *1/f*=0.33 for Figure 2.11.b. These values are very close, making it difficult to distinguish the images on the basis of 1/f values. However, a close look at the DFT spectrum in Figure 2.13.b reveals the existence of a second peak with a frequency of $f_2 = 1.42$. This frequency implies that Figure 2.11.b contains another texture of mean size 0.70, while Figure 2.11.a is well-represented by only 1 texture.

## Another example of polymeric structures

This is the case of a typical polymeric porous structure. Figure 2.14 illustrates a porous film with a square size [140×140] obtained by scanning laser microscope. Pores with various sizes and shapes are present in the SEM film (Sarazin & Favis, 2003) of 50/50 poly-(L-lactide) (PLLA)/polystyrene (PS) blends with polystyrene-b-poly-L-lactide (PS-b-PLLA) copolymer concentration of 8%, based on the weight of the polystyrene.
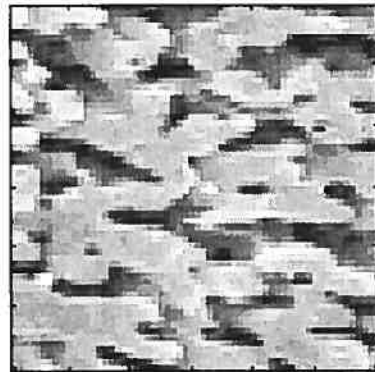


**Figure 2.14: 50/50 PLLA/PS blends with PS-b-PLLA copolymer concentration of 8%, based on weight of the polystyrene**

The aim here is to investigate the impact of the threshold in analyzing grey level images, using our method. We want to verify if the main peak in the DFT signal is stable and independent of the threshold value, and eventually to find out if there is a threshold value which is more suited to reveal the most pertinent features of an image.

To accomplish this, we consider 2 approaches. In the first approach, we conduct the analysis with different individual thresholds. The second is done by applying the whole threshold spectrum and then taking the mean characteristic values. This is explained in detail in the following pages.

- **First approach**

In this approach, we consider different threshold values to estimate frequency and porosity. The results with threshold values of 100, 127, 150, and 200 are shown in Table 4. The derived autocorrelation functions of binary images, for each chosen threshold, along with their corresponding DFT spectra appear in Figures 2.15 and 2.16, respectively. The DFT graphs of the oscillation signals in Figure 2.15 manifest several peaks referring to different complex patterns embedded in the image.

| Threshold | 110 | 127 | 150 | 200 | 250 |
|-----------|-----|-----|-----|-----|-----|
| $f_1$ | 1.04 | 1.04 | 1.00 | 3.116 | - |
| Slope | -0.7966 | -0.7116 | -0.4278 | -0.0437 | 0 |
| $\phi$ | 0.7278 | 0.6256 | 0.3050 | 0.0086 | 0 |

Table 4: Porosity, slope and frequency in different thresholds of Figure 2.14

The related frequency of each peak is presented in Table 5. It can be seen that as the threshold increases, porosity, and hence the slope values of the autocorrelation function spectrum, decreases. With the change of threshold, no significant modulation of frequency of main peak $f_1$, peak number 1, is observed (except for threshold = 200).

As is obvious in DFT spectra, the position of main peak $\mathbf{f_1}$ in thresholds 110, 127 and 150 does not change very much and has values of $f_1=1.03$, $f_1=1.04$ and $f_1=1.00$, respectively, indicating that there is a predominant feature represented by this frequency, which is less sensitive to the thresholding process. A shift to the frequency value of $f=3.11$ is observed when the threshold is equal to 200. This can be expected since the image can change dramatically with high threshold values. Hence, there is a range in which we can have a kind of stability of the estimated characteristic values of the image.
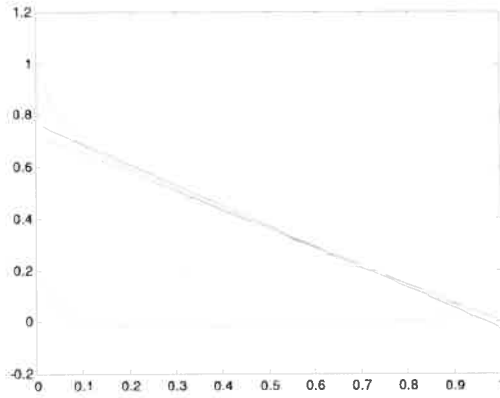
**Threshold=110**
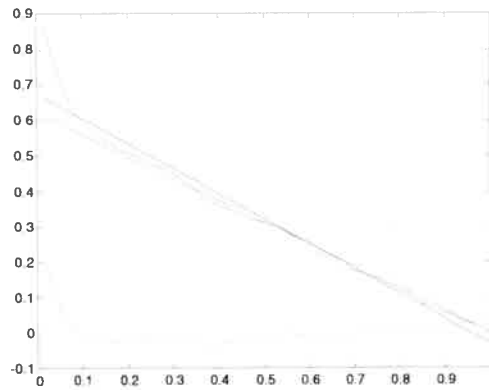


**Threshold=127**
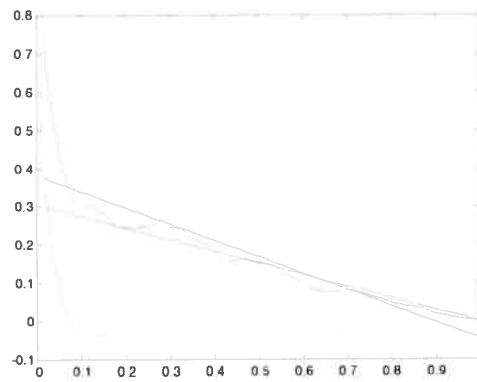


**Threshold=150**

**Figure 2.15: The autocorrelation function spectrum of Figure 2.14 in various thresholds**

**Threshold=110**



**Threshold =127**



**Threshold =150**



**Figure 2.16: The DFT spectrum of Figure 2.15 in various thresholds**

|              | $f_1$ | $f_2$ | $F_3$ | $f_4$ | $f_5$ |
| ------------ | ----- | ----- | ----- | ----- | ----- |
| Threshold 110 | 1.04 | 2.22 | 3.25 | 4.26 | 5.40 |
| Threshold 127 | 1.04 | 2.19 | 3.30 | 4.23 | 5.40 |
| Threshold 150 | 1.00 | 2.22 | 3.26 | 4.21 | 5.46 |

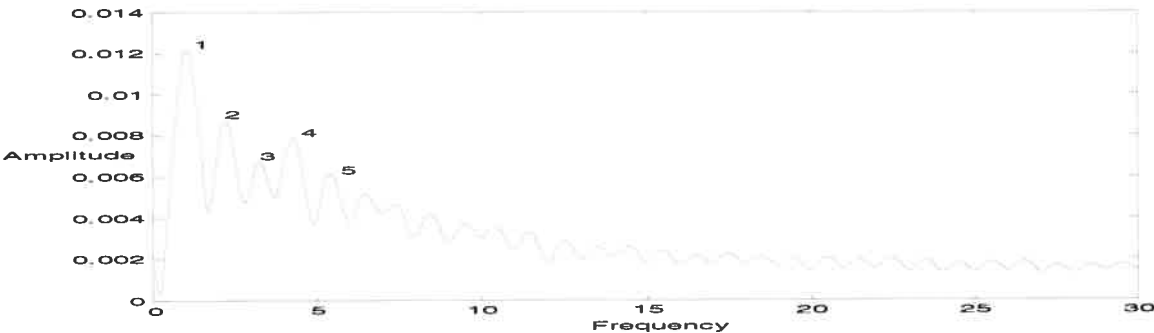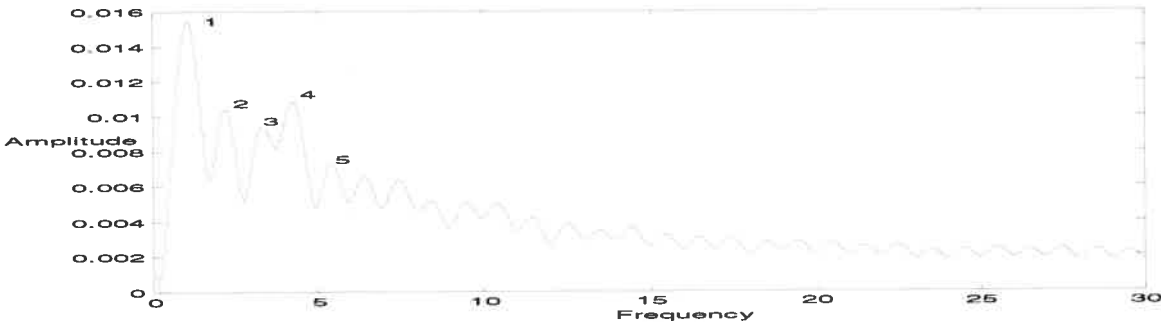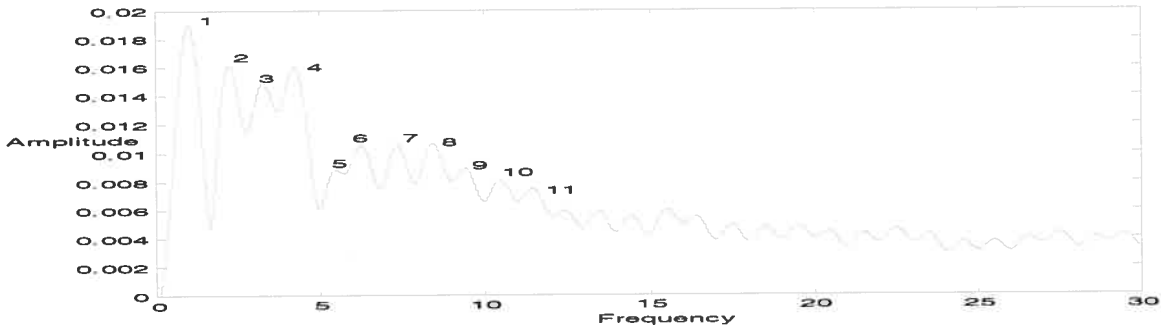Table 5: The related value of frequency for the first 5 peaks in the DFT spectrum of Figure 2.16

## ▪ Second approach

We used whole threshold values, that is, from 0 to 255, and then took the mean value of its autocorrelation function spectrum. Figure 2.18 refers to the DFT spectrum which is applied to the obtained autocorrelation function spectrum shown in Figure 2.17. The idea behind this approach is to allow identification of a preferential frequency related to the whole range of thresholds.

|             | $f_1$ | $1/f_1$ | $f_2$ | $1/f_2$ | $f_3$ | $1/f_3$ | $f_4$ | $1/f_4$ | $f_5$ | $1/f_5$ |
| ----------- | ----- | ------- | ----- | ------- | ----- | ------- | ----- | ------- | ----- | ------- |
| Figure 2.18 | 1.03  | 0.97    | 2.22  | 0.45    | 3.27  | 0.31    | 4.24  | 0.24    | 5.40  | 0.19    |

Table 6: Various frequencies of the DFT spectrum corresponding to Figure 2.18

The DFT spectrum in Figure2.18 illustrates several predominant peaks in terms of amplitude, and the measured values of frequency of the first 5 peaks are shown in Table 6. The first peak with $f_1$=1.03 refers to the main peak in terms of amplitude. Indeed, we found out that considering the position of the other peaks as well yields a good match with the resulting DFT spectrum of thresholds 110 and 127.
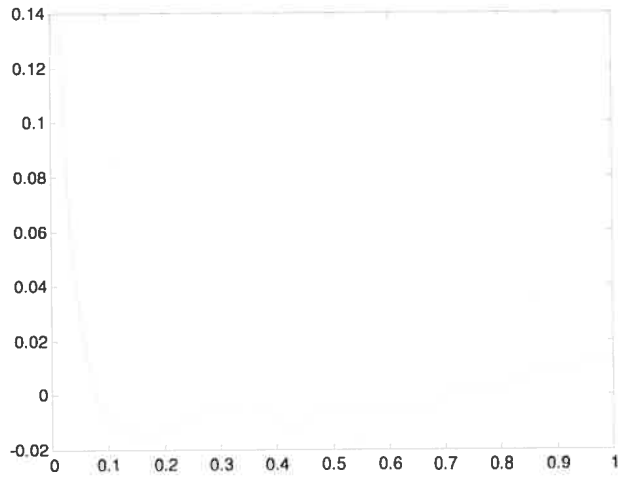
**Figure 2.17: The autocorrelation function spectrum of Figure 2.14 with the whole threshold**
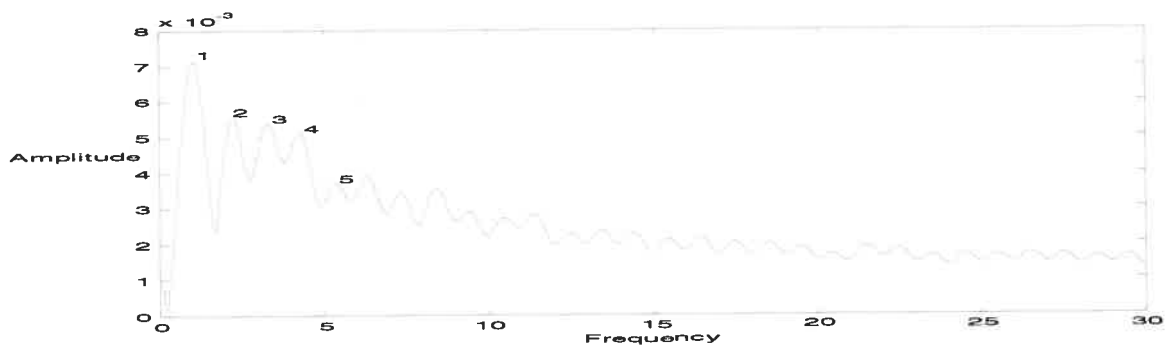


**Figure 2.18: The DFT spectrum of Figure 2.17**

**To summarize, the steps of the developed method can be described as follows:**

---

### *Main steps of the method*

---

- Use binary images (real or synthesized)
- Apply the autocorrelation function (ACF) to these images to obtain a spectrum
- Decompose the spectrum into components: "slope" and "oscillation curve"
- Calculate the porosity of structures using the porosity formula
- Estimate the slope of the autocorrelation function spectrum of the image using the least mean squares (LMS)
- Establish the equivalence between the slope of the autocorrelation function spectrum and the calculated porosity
- Withdraw the slope from the autocorrelation function spectrum to complementary information
- Evaluate the remaining oscillation part of the spectrum with the DFT
- Extract frequencies from the DFT spectrum obtained
- Relate frequency to the number of strips in the image
- Relate the inverse of frequency to the width of the strips

---

# CHAPTER 3: CONCLUSION

Synthetic polymer design has been revolutionized recently by new achievements in high-resolution characterization tools, such as broad-mass-range spectrometry. These new measurement technologies make it possible to gain access to finer details of structures, so that more sophisticated data analysis is needed (Nekka & Li, 2004). As a matter of fact, the experimental signals obtained are generally very complex, requiring the development of more advanced mathematical tools for their analysis. For example, the high-resolution mass spectra of synthetic polymers can contain a large number of peaks, implying that these spectra cannot be considered in the traditional continuum way (Nekka & Li, 2004). This calls for more appropriate and powerful analytical methods. The autocorrelation function has been proposed to handle complex time series (Wallace & Guttman, 2002). Its Fourier transform, known as the structure factor, is used in polymer characterization by light scattering experiments to indicate which wave vector components are present in the autocorrelation function (Teraoka, 2002).

Hence, the requirement to characterize the structure of porous solids arises in a number of fields, such as catalyst recovery filters (Ejaz et al., 2001), polymeric drug delivery systems (Brown et al., 1986; Ouriemchi & Vergnaud, 2000; Kim et al., 2004), and bone diseases (Ripamonti, 1996; Ambrosio et al., 2001), to name a few.

Despite recent progress in accurate characterization equipment for the measurement of these parameters, there is still no robust method that can distinguish porous structures exhibiting the same porosity or other geometric parameters, such as fractal dimension and lacunarity (Nekka & Li, 2003a).

This study is part of an ongoing effort to investigate polymeric porous materials to provide means that reveal the structural information of bi-phase thread-like textures. We have favored an approach based on the widely-used autocorrelation function. The latter, which is a particular case of the correlation function, has been applied mainly in signal analysis and spectrometry for several types of mass spectra.

We showed in this work that the autocorrelation function can be investigated differently in the context of spatial signals (in parallel to the classical time series context)

and more deeply to be related to the usual image parameters, such as porosity. We have come up with 2 independent parameters, defined through the "slope" and "oscillation" parts of the autocorrelation function. The slope has been proved experimentally to give a close estimation of porosity. A theoretical proof of the correspondence between porosity and the LMS slope of the autocorrelation function has been provided by Nekka et al. (2005) for typical cases of porous media.

It is worthwhile reiterating that when dealing with more complex textures, the autocorrelation function is more irregular, making it difficult to use the FT. In such cases, as illustrated by fat fractals, a different approach has to be applied (Nekka et al., 2005).

In even more complex cases, porosity degenerates in an additional sense: it can also be zero or infinite, as is the case for (thin) fractal sets. For these sets of zero Lebesgue measure, we have to completely reformulate the autocorrelation function to make it applicable to this case, which has been done recently by Nekka et al. (2004).

Hence, one cannot hope for an almighty solution for all textures (one fits all!). For different texture complexities, different strategies have to be adopted.

The method developed was motivated by the study of texture (micro-texture), employing more advanced mathematical methods. The autocorrelation function has been used traditionally to measure the similarity of sample distribution (Griffith, 1987; Glenny, 1992; Nekka & Li, 2004). In the present work, we develop a new analytical approach of the autocorrelation function to extract 2 independent components, which we relate to porosity as well as to pore frequency and extent. Indeed, in a first step, we have experimentally shown, on real images, how a relationship does exist between porosity and the least mean squares slope of the autocorrelation function. In a second step, we have subtracted this least mean squares slope from the autocorrelation function to keep the information hidden in the oscillating part, thus excluding porosity. On the remaining curve, a Fourier transform has been applied to obtain the main frequency components of the image that reflect the number of periodic patterns as well as width.

We have shown in this work that classical mathematical methods can be revisited in new ways to probe fine texture. The optimization procedure presented here is in its infancy. Its potential has to be explored further to make it applicable in more general cases. The originality of our work lies in the new analytical approach of the

autocorrelation function. To the best of our best knowledge, it is the first time that the autocorrelation function has been used in this way within a geometric context.

# Bibliography

**Allain, C., Cloitre, M.,** *Characterizing the lacunarity of random and deterministic fractal sets,* Phys. Rev. A, 44, 1991, 3552-3558.

**Ambrosio AM, Sahota JS, Khan Y, Laurencin CT,** *A novel amorphous calcium phosphate polymer ceramic for bone repair: I. Synthesis and characterization.* J. Biomed Mater Res, 58, 2001, 295-301.

**Avnir, D., Farin, D., Pfeifer, P.,** *Surface geometric irregularity of particulate materials: the fractal approach,* J. Colloid Interface Sci., 103, 1985, 112-123.

**Berryman, J.G.,** *Relationship between specific surface area and spatial correlation functions for anisotropic porous media,* J. Math. Phys., 28, 1987, 244-245.

**Bracewell, R.N.,** *The Fourier Transform and Its Applications,* New York: McGraw-Hill Book Company, 1965.

**Bourke, P.,** *DFT (Discrete Fourier Transform). FFT (Fast Fourier Transform),* 1993, http://astronomy.swin.edu.au/~pbourke/other/dft/

**Brown, L., Siemer, L., Munoz, C., Langer, R.,** *Controlled release of insulin from polymer matrices. In vitro kinetics,* Diabetes, 35, 1986, 684-691.

**Bulgakov, S.A., Konotop, V.V.,** *Peculiarities of wave scattering by fat fractals,* Phys. Rev. A, 46, 1992, 8024-8027.

**Butler, J.P., Mair, R.W., Hoffmann, D., Hrovat, M.I., Rogers, R.A., Topulos, G.P., Walsworth, R.L., Patz, S.,** *Measuring surface-area-to-volume ratios in soft porous materials using laser-polarized xenon interphase exchange nuclear magnetic resonance,* J. Phys. Condens. Matter 14, 2002, L297-L304.

**Carman, P.C.,** *Flow of Gases Through Porous Media,* London: Butterworth, 1956.

**Champeney, D.C.,** *Fourier Transforms and Their Physical Applications,* New York: Academic Press, 1973, 498.

**Cooley, J. W., Tukey, J. W.,** *An algorithm for the machine calculation of complex Fourier series,* Math. Comput. 19, 1965, 297–301.

**Ejaz, M., Tsujii, Y., Fukuda, T.,** *Controlled grafting of a well-defined polymer on a porous glass filter by surface-initiated atom transfer radical polymerization,* Polymer, 42, 2001, 6811-6815.

**Freude, D., Karger, J.,** *NMR techniques.* In: F. Schuth. K.S.W. Sing and J. Weithkamp (eds.), *Handbook of Porous Solids*, Weinheim: Wiley VCH, 1, 2002, 465-504.

**Glenny, R.W.,** *Spatial correlation of regional pulmonary perfusion*, J. Appl. Physiol., 72, 1992, 2378-2386.

**Gouyet, J.F.,** *Physique et structures fractales.* Paris: Masson, 1992.

**Griffith, D.A.,** *Spatial Autocorrelation: A Primer.* Washington, DC: Association of American Geographers, Resource Publications in Geography, 1987.

**Hilfer, R.,** *Transport and relaxation phenomena in porous media,* Advances in Chemical Physics XCII, 1996, 299-424.

**Hilfer, R.,** *Review on scale dependent characterization of the microstructure of porous media,* Transport in Porous Media, 46, 2002, 373-390.

**Hilfer R., Manwart C.,** *Permeability and conductivity for reconstruction models of porous media*, Phys. Rev., 64, 2001, 021304-4.

**Huang, Y.J., Lu, S.Z.,** *A measurement of the porosity in aluminium cast alloys using fractal analysis,* Proc. 2nd International Aluminum Casting Technology Symposium, ASM, 2002.

**Hunt, A.G.,** *Percolative transport in fractal porous media,* Chaos, Solitons and Fractals, 17, 2003, 309-325.

**Kai, Z., Ying, D., Guo-Qiang, C.,** *Effect of surface morphology on the biocompatibility of the polyhydroxyalkanoates,* Biochem. Eng. J. 16, 2003, 115-123.

**Kim, H.W., Knowles, J.C., Kim, H.E.,** *Hydroxyapatite/poly($\varepsilon$-caprolactone) composite coatings on hydroxyapatite porous bone scaffold for drug delivery*, Biomaterials, 25, 2004, 1279-1287.

**Krohn, C.E., Thompson, A.H.,** *Fractal sandstone pores: automated measurements using scanning-electron-microscope images*, Phys. Rev. B, 33, 1986, 6366-6374.

**Lee, Y.M., Shim, J.K.,** *Preparation pH/temperature responsive polymer membrane by plasma polymerization and its riboflavin permeation,* Polymer 38, 1997, 1227-1232.

Li, J., Arneodo, A., Nekka, F., *A practical method to experimentally evaluate the Hausdorff dimension: an alternative phase-transition-based methodology*, Chaos, 14, 2004, 1004-1017.

Lowell, S., Shields, J.E., *Powder Surface Area and Porosity*, 3$^{rd}$ edition, New York: Chapman and Hall, 1991.

Markov, K.Z., Willis, J.R., *On the two-point correlation function for dispersions of nonoverlapping spheres*, Mathematical Models and Methods in Applied Sciences, 8, 1998, 359-377.

Mandelbrot, B.B., *The Fractal Geometry of Nature*, San Francisco: Freeman, 1982.

Nekka, F., Li, J., *The Hausdorff measure functions: a new way to characterize fractal sets*, Recognition Lett., 24, 2003a, 2723-2730.

Nekka, F., Li, J., *A continuous translation based method to reveal the fine structure of fractal sets*, Arabian Journal for Science and Engineering, 28, 2003b, 169-188.

Nekka, F., Li, J., *Characterization of fractal structures through a Hausdorff measure based method*, In: M.M. Novak (ed.), *Thinking in Patterns, Fractals and Related Phenomena in Nature*, World Scientific, 2004, 213-221.

Nekka, F., Li, J. *A new analysis approach to porous media texture – Mathematical tools for signal analysis in a context of increasing complexity*, Certain Mathematical Topics in Real World Problems, Furati, K.M et al. (Edts), 2004, 373-388.

Nekka, F., Li, J., *Various mathematical approaches to extract information from textures of increasing complexities*, In *Fractals in Engineering*, Springer-Verlag, J. Lévy Véhel and E. Lutton (Edts.), 2005, 255-270.

Ouriemchi, E.M., Vergnaud, J.M., *Processes of drug transfer with three different polymeric systems with transdermal drug delivery*, Computational and Theoretical, Polymer Sci., 10, 2000, 391-401.

Pachence, J.M., *Collagen based device for soft tissue repair*, J. Biomed. Mater. Res. (Appl. Biomater.), 33, 1996, 35-40.

Partt, M.A., *Digital signal processing, Xavier University of Louisiana*, 2002, http://webusers.xula.edu/mpratt/csce4320/1.

Pinnau, I., Hellums, M.W., Koros, W.J., *Gas transport through homogeneous and asymmetric polyestercarbonate membranes*, Polymer, 32, 1992, 2612.

**Rijniers, L.A., Magusin, P.C., Huinink, H.P., Pel, L., Kopinga, K.,** *Sodium NMR relaxation in porous materials,* J. Magn. Reson., 167, 2004, 25-30.

**Ripamonti, U.,** *Osteoinduction in porous hydroxyapatite implanted in heterotopic sites of different animal models,* Biomaterials, 17, 1996, 31-35.

**Risbud, M.V., Hardikar, A.A., Bhat, S.V., Bhonde, R.,** *pH-sensitive freeze-dried chitosan-polyvinyl pyrrolidone hydrogels as controlled release system for antibiotic delivery,* J. Control Release, 68, 2000, 23-30.

**Salonen, J., Björkqvist, M., Laine, E.,** *Comparison of different methods in micro-structural characterization of porous silicon,* J. Appl. Cryst. 33, 2000, 504-506.

**Sarazin, P., Favis, B.D.,** *Morphology control in co-continuous poly (L-lactide)/polystyrene blends: a route towards highly structured and interconnected porosity in poly (L-lactide) materials,* Biomacromolecules, 4, 2003, 1669-1679.

**Shibata, H., Shioya, N., Kuroyanagi, Y.,** *Development of new wound dressing composed of spongy collagen sheet containing dibutyryl cyclic AMP,* J. Biomater. Sci. Polym. Edn., 8, 1997, 601–621.

**Smith, T.G., Jr., Lange, G.D., Marks W.B.,** *Fractal methods and results in cellular morphology -- dimensions, lacunarity and multifractals,* J. Neurosci. Methods, 69, 1996, 123-136.

**Teraoka, I.,** *Polymer Solutions: An Introduction to Physical Properties.* New York: Wiley-Interscience, 2002.

**Thomas, J.J., Jennings, H.M., Allen, A. J.,** *The surface area of hardened cement paste as measured by various techniques,* Con. Sci. Eng., 1, 1999, 45-64.

**Umberger, D.K., Farmer J.D.,** *Fat fractals on the energy surface,* Phys. Rev. Lett., 55, 1985, 661–664.

**Wallace, W.E., Guttman, C.M.,** *Data analysis methods for synthetic polymer mass spectrometry: autocorrelation,* J. Res. Natl. Inst. Technol., 107, 2002, 1-17.

**Washburn, E.W.,** The *dynamics of capillary flow,* Phys. Rev., 17, 1921, 273-283.

**Wu, J.,** *The interfacial properties and porous structures of polymer blends characterized by synchrotron small-angle X-ray scattering,* Polymer 44, 2003, 8033-8040.

**Xu, Y.F., Sun, D., Yao, Y.P.,** *Surface fractal dimension of bentonite and its application to determination of swelling properties*, Chaos, Solitons and Fractals, 19, 2004, 347-356.

**Yu, M., Li, J.H.,** *Some fractal characters of porous media*, Fractals, 9, 2001, 365-372.

**Yu, B., Cheng, P.,** *A fractal permeability model for bi-dispersed porous media*. Int. J. Heat and Mass Transfer 4, 2002, 2983-2993.

**Zeng, M., Fang, Z., Xu, C.,** *Effect of compatibility on the structure of the microporous membrane prepared by selective dissolution of chitosan/synthetic polymer blend membrane,* J. Membrane Sci., 230, 2004, 175-181.

**Web sites reference:**

**I.** Porosity, Specific Yield & Capillary Rise, Laboratory 1, HWR 431/531
http://quebec.hwr.arizona.edu/classes/hwr431/Lab1.pdf.